

1 **Projected future changes in cryosphere and hydrology of a mountainous**
2 **catchment in the Upper Heihe River, China**

3

4 Zehua Chang ¹, Hongkai Gao ^{1*}, Leilei Yong ¹, Kang Wang ¹, Rensheng Chen ²,
5 Chuntan Han ², Otgonbayar Demberel ³, Batsuren Dorjsuren ⁴, Shugui Hou ⁵, Zheng
6 Duan ⁶

7 ¹ Key Laboratory of Geographic Information Science (Ministry of Education of
8 China), School of Geographical Sciences, East China Normal University, Shanghai,
9 [ChinaChina](#)

10 ² Qilian Alpine Ecology and Hydrology Research Station, Key Laboratory of
11 Ecohydrology of Inland River Basin, Northwest Institute of Eco-Environment and
12 Resources, Chinese Academy of Sciences, Lanzhou 730000, China

13 ³ Department of Geography and Geology Khovd branch of National University of
14 Mongolia, Erkh choolonii street, Khovd, Mongolia

15 ⁴ Department of Environment and Forest Engineering, National University of
16 Mongolia, Ulaanbaatar 210646, [84140](#), Mongolia

17 ⁵ School of Oceanography (SOO), Shanghai Jiao Tong University (SJTU), Shanghai,
18 China

19 ⁶ Department of Physical Geography and Ecosystem Science, Lund University,
20 Sölvegatan 12, SE-223 62, Lund, Sweden

21 *Correspondence: Hongkai Gao (hkgao@geo.ecnu.edu.cn)

22

23 **Abstract:** Climate warming exacerbates the degradation of the mountain cryosphere,
24 including glacier retreat, ~~reduction in snow cover area, and~~ permafrost degradation

25 [and snow cover reduction](#). These changes dramatically alter the local and downstream
26 hydrological regime, posing significant threats to basin-scale water resource
27 management and sustainable development. However, [therethis issue](#) is still ~~a lack of~~
28 ~~systematic research~~[not adequately addressed, particularly that evaluates the variation](#)
29 ~~of cryospheric elements~~ in mountainous catchments ~~and their impacts on future~~
30 ~~hydrology and water resources~~. ~~In this study, w~~We developed an integrated cryospheric-
31 hydrologic model, ~~referred to as the~~ FLEX-Cryo model. ~~This model to~~
32 comprehensively considers glaciers, snow cover, frozen soil, and their dynamic impacts
33 on hydrological processes. ~~Taking in~~ the mountainous Hulu catchment located in the
34 Upper Heihe river of China ~~as a case, w~~We utilized the state-of-the-art climate change
35 projection data [under two scenarios \(SSP2-4.5 and SSP5-8.5\)](#) from the sixth phase of
36 the Coupled Model Intercomparison Project (CMIP6) to simulate the future changes in
37 the mountainous cryosphere and their impacts on hydrology. Our findings showed that
38 ~~the two glaciers in the Hulu catchment will completely melt out around the years 2045–~~
39 ~~2051. By~~[under the medium \(SSP2-4.5\) and high emission scenario \(SSP5-8.5\), by](#) the
40 end of the 21st century, [the glacier will completely melt out around the years 2051 and](#)
41 [2045, respectively.](#) The annual maximum snow water equivalent is projected to
42 decrease by 41.4% and 46.0%, while the duration of snow cover will be reduced by
43 approximately 45 and 70 days. The freeze onset of ~~seasonal frozen soil~~[seasonally frozen](#)
44 [soil](#) is expected to be delayed by 10 and 22 days, while the thaw onset of permafrost is
45 likely to advance by 19 and 32 days. Moreover, the maximum freeze depth of ~~seasonal~~
46 ~~frozen soil~~[seasonally frozen soil](#) is projected to decrease by 5.2 and 10.9 cm per decade,
47 and the depth of the active layer will increase by 8.2 and 15.5 cm per decade. Regarding
48 hydrology, [catchment total](#) runoff exhibits a decreasing trend ~~until~~[and](#) the ~~complete~~

49 ~~melt-out~~ tipping point of glaciers, resulting in a total runoff decrease of 15.6% and
50 18.1%. Subsequently, total runoff shows an increasing trend, primarily due to an
51 increase in precipitation. glacier runoff occur approximately between 2019 and 2021.
52 Permafrost degradation ~~causes~~ will likely reduce the duration of low runoff in the early
53 thawing season ~~to decrease, and,~~ the discontinuous baseflow recession gradually
54 transitions into linear recessions, ~~leading to an~~ and the increase ~~in~~ of baseflow. Our
55 results highlight the significant changes expected in the mountainous cryosphere and
56 hydrology in the future. These findings enhance our understanding of cold-region
57 hydrological processes and have the potential to assist local and downstream water
58 resource management in addressing the challenges posed by climate change.

59 **Keywords:** Glacier, Snow cover, ~~Seasonal frozen soil~~ Seasonally frozen soil,
60 Permafrost, Runoff, Model prediction

61

62 1. Introduction

63 “How will cold region runoff and groundwater change in a warmer climate?” was
64 identified by the International Association of Hydrological Sciences (IAHS) as one of
65 the 23 unsolved scientific problems (Blöschl et al., 2019). The mountain cryosphere,
66 which includes glaciers, snow cover, and frozen soil in high-altitude regions, has a
67 significant impact on water resources (Adler et al., 2019; Arendt et al., 2020; Rasul et
68 al., 2020; Zhang et al., 2022). The Mm mountain cryosphere is considered a crucial "water
69 tower" and a climate change indicator due to its sensitivity to climate change (Tang et
70 al., 2023). However, the cryosphere is rapidly retreating in many parts of the world,
71 including glacier retreat, expansion of glacier lakes, northward movement of the
72 permafrost southern limit, and shrinking snow cover area (Moreno et al., 2022; S. Wang

73 et al., 2022; Ding et al., 2019; Wang et al., 2023). These changes have disrupted the
74 water tower region and pose significant challenges to sustainable water resources
75 management (Ragettli et al., 2016; Yao et al., 2022).

76 The degradation of the mountain cryosphere varies from region to region
77 (Andrianaki et al., 2019; Wang et al., 2019). Lower altitudes experience a decreasing
78 trend in snow cover days, snow depth, snow water equivalent, and snowmelt due to
79 climate warming, while higher altitudes present a more complex picture (Connon et al.,
80 2021; Nury et al., 2022; Yang et al., 2022). Global continental glacier mass balance
81 from 2006 to 2015 was approximately -123 ± 24 GT yr⁻¹, with significant losses
82 observed in the Southern Andes, Caucasus Mountains, and Central Europe, while the
83 Karakoram and Pamir regions exhibited lesser loss (Intergovernmental Panel on
84 Climate Change (IPCC), 2022; Van Der Geest and Van Den Berg, 2021). Future
85 projections suggest a 40% decrease in global permafrost by the end of the century,
86 potentially transitioning into ~~seasonal frozen soil~~[seasonally frozen soil](#) (Chadburn et al.,
87 2017); [Martin et al., 2023](#)). The mountain cryosphere serves as a significant freshwater
88 reservoir, impacting water resources and the hydrological cycle (Ding et al., 2020).

89 In a warming climate, ~~glacier runoff~~ exhibits a "tipping point" characterized by
90 an initial increase followed by a subsequent decline (Rosier et al., 2021; Zhang et al.,
91 2012). While small glaciers have already experienced this tipping point, its occurrence
92 in large glaciers remains uncertain (Brovkin et al., 2021; Huss and Hock, 2018).
93 Permafrost degradation leads to an increase in active layer thickness, resulting in the
94 melting of subsurface ice and an augmentation of soil water storage capacity
95 (Abdelhamed et al., 2022). Additionally, the degradation of the cryosphere significantly
96 impacts the atmosphere, biosphere, surface energy balance, ecological water use, and

97 ecosystems (Gilg et al., 2012; Miner et al., 2022; Pothula and Adams, 2022).
98 Understanding the complex interactions between cryosphere degradation and
99 ecosystems is crucial, but quantitatively observing the degradation process in high-
100 altitude regions is challenging. Hydrological models provide an effective approach to
101 analyze degradation patterns and assess the impact on future water resources (Han and
102 Menzel, 2022).

103 Glacio-hydrology is influenced by both glacier melt and glacier dynamics. Glacier
104 melting models can be categorized into three types: energy balance, temperature index,
105 and hybrid models (He et al., 2021; Gao et al., 2021; Negi et al., 2022; Zekollari et al.,
106 2022). While energy balance models analyze glacier accumulation and melt processes
107 based on solid physical mechanisms, they require extensive forcing data that may not
108 be readily available in mountainous regions (Huss et al., 2010). ~~On the other hand~~In
109 contrast, temperature index models are simpler and more effective, requiring fewer
110 parameters (including degree-day factor and threshold temperature) and forcing data
111 (temperature and precipitation) (Bolibar et al., 2022; Vincent and Thibert, 2023). These
112 models~~It~~ performs well at both daily and monthly scales. Glaciers ~~are moving~~ing slowly,
113 due to the combined effects of gravity and high viscosity of ice. Due to climate change,
114 ice becomes thinner, and glacier loses its mass balance, which will cause the glacier
115 morphology to evolve to a new balance status. Glacier dynamic models, with full-
116 Stokes approach as the most complete form, and many other simplifications, such as
117 the shallow-ice approximation, and the shallow-shelf approximation~~ete~~, are still
118 computationally expensive, hindering their implications in large scale studies. Three
119 conceptual models are commonly used for glacier evolution: volume-area scaling (V-
120 A) method, accumulation area ratio (AAR) method, and Δh -parameterization (Michel

121 et al., 2022; Wiersma et al., 2022). The first two approaches do not consider the detailed
122 changes in different elevation bands, while the Δh -parameterization approaches only
123 require glacier mass balance as forcing data to analyze changes in ice thickness at
124 different elevation bands based on the relationship between glacier mass balance and
125 glacier area (Huss et al., 2010). The temperature index method coupled with the Δh -
126 parameterization approach serves as an effective module to simulate glacier evolution
127 and its impacts on hydrology.

128 Permafrost hydrology models can be classified into one-dimensional models and
129 distributed watershed models (Elshamy et al., 2020). One-dimensional hydrological
130 models, such as the Stefan equation, the temperature at the top of permafrost (TTOP)
131 model, CoupModel, and SHAW model, are effective in simulating freeze depth,
132 hydrothermal transport, and carbon or nitrogen transport, but they are unable to capture
133 the broader impact of permafrost on hydrology at catchment scale (Kaplan Pastíriková
134 et al., 2023; Li et al., 2022; Liu et al., 2023). On the other hand, distributed watershed
135 models, such as the Cold Regions Hydrological Model (CRHM), Hydrogeosphere
136 (HGS), and Distributed water-heat coupled model (DWHC), consider the spatial
137 variability of permafrost properties and simulate the interactions between permafrost,
138 surface water, and groundwater (Chen et al., 2008; He et al., 2023; Pomeroy et al.,
139 2022). These models operate on a small-scale basis and require extensive prior
140 knowledge, following a "bottom-up" approach that relies on small-scale field
141 observations and situational models to comprehend the effects of permafrost on
142 hydrology (Peng et al., 2016). However, the freeze-thaw cycle is influenced by multiple
143 interconnected factors, including climate, topography, slope orientation, snowpack, and
144 vegetation (Chang et al., 2022). The process of upscaling would lead to the neglect of

145 some variables and the amplification of others (Fenicia and McDonnell, 2022). In
146 contrast, the FLEX-Cryo model is based on the FLEX-Topo-FS model, which employs
147 a "top-down" modeling procedure that involves observed data analysis, qualitative
148 perceptual modeling, quantitative conceptual modeling, and the testing of model
149 realism. This model exhibits the ability to accurately and expeditiously identify key
150 elements in permafrost hydrological processes and then simulate hydrology at the
151 catchment scale (Beven, 2012; Gao et al., 2022).

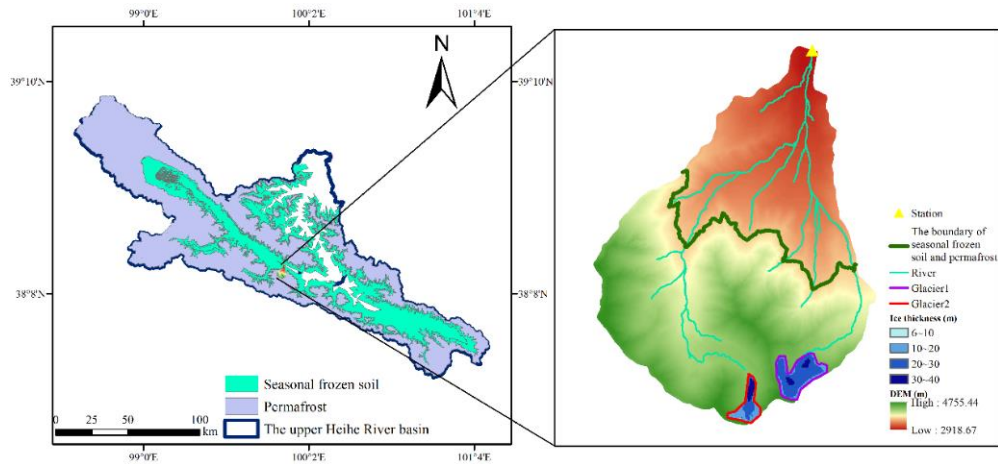
152 The aim of this study is to integrate the FLEX-Topo-FS model and a glacier
153 evolution model (Δh -parameterization) to develop a landscape-based model of the
154 mountain cryosphere, referred to as FLEX-Cryo. This model will be utilized to simulate
155 changes in various components of the mountain cryosphere and evaluate their impacts
156 on hydrological processes, thereby enhancing our understanding of the hydrological
157 cycle. The model will be driven by eight bias-corrected Global Climate Models (GCMs)
158 under SSP2-4.5 and SSP5-8.5 scenarios obtained from the Coupled Model
159 Intercomparison Project Phase 6 (CMIP6), which will be used to predict future changes
160 in glaciers, snow, and frozen soil, as well as their effects on hydrology.

161 **2. Study area and data**

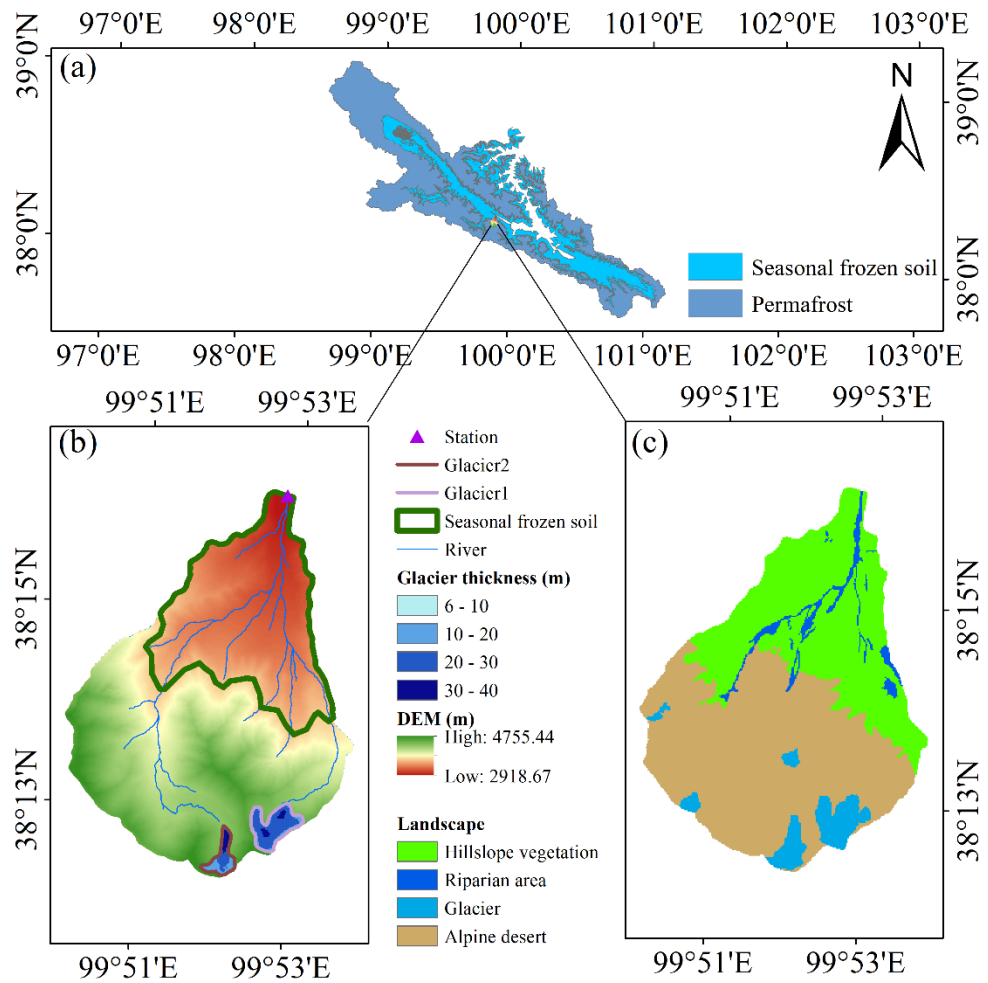
162 **2.1 Study area**

163 The Hulu catchment is located in the upper reaches of Heihe River basin ($38^{\circ} 12'$
164 $N-38^{\circ} 17' N$, $99^{\circ} 50' E-99^{\circ} 53' E$) and about 23.1 km^2 . The elevation ranges
165 from 2960-4820m. The Hulu catchment belongs to continental monsoon climate.
166 Rainfall is the major phase of precipitation, and there is also snowfall in the winter.
167 Four landscapes are identified, i.e. glacier (5.6%), alpine desert (53.5%), vegetation
168 hillslope (37.5%), and riparian zone (3.4%; Fig. 2-1(c)). The landscape pattern in Hulu

169 catchment has typical altitude zonality. The vegetation and riparian are almost
 170 distributed in the lower elevation bands. Alpine desert, and glacier are in the high
 171 elevation bands. There is almost no human activity in the catchment- ([Liu and Chen,](#)
 172 [2016; Li et al., 2014](#)). There are two [major](#) glaciers, i.e. Glacier1 and Glacier2 (Fig.1
 173 [\(b\) and Fig.2](#)) in the catchment. And the Galcier1 was also named as the Shiyi Glacier
 174 in the glacier catalogue of China. ~~Seasonal frozen soil~~[Seasonally frozen soil](#) and
 175 permafrost both exist in the catchment. The lower limit of permafrost is around in 3650-
 176 3700 m. Permafrost region account for 64% of the total catchment and the others are
 177 ~~seasonal frozen soil~~[seasonally frozen soil](#). The soil generally starts to freeze in the
 178 October- ([Gao et al., 2019](#)). Thus October 1 was set as the start of hydrological year, so
 179 forth. All the interannual variations in this study were based on the hydrology year.

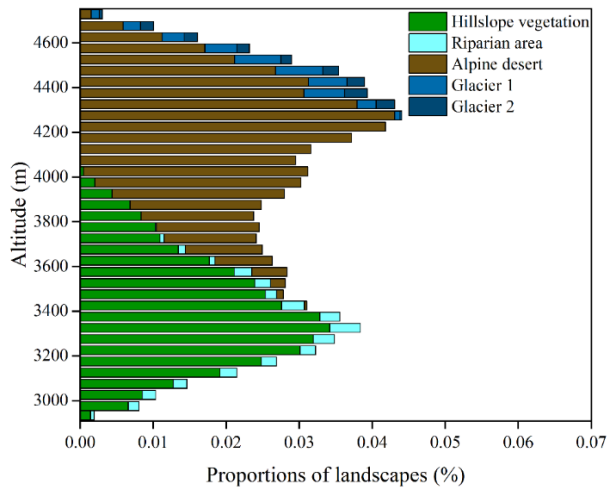


180
 181
 182

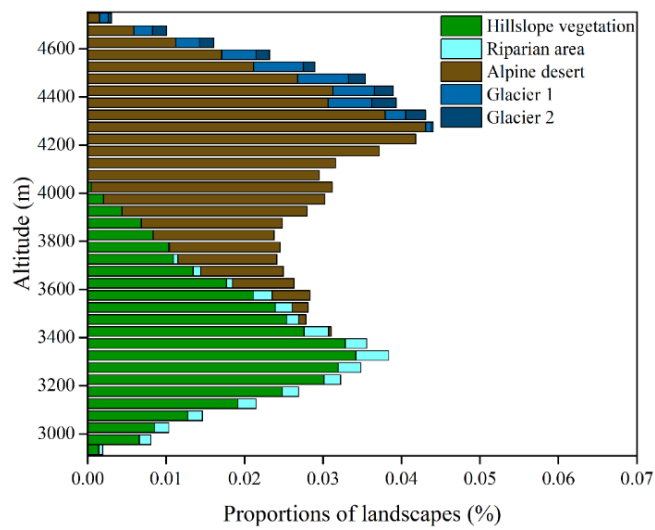


183

184 Figure 1. (a) The distribution of permafrost and seasonally frozen soil on the
 185 upper Heihe River basin, and the location of Hulu catchment. (b) The digital elevation
 186 model, and the thickness of the two major glaciers. (c) Spatial distribution of four
 187 landscapes (glacier and the location of study area, alpine desert, vegetation hillslope,
 188 and riparian zone)



189



190

191 Figure 2. Landscape classification at different elevation bands

192 **2.2 Data**

193 Temperature and precipitation are observed at 2920 m, near the outlet of the
 194 catchment, from [January 1, 2011 to December 31, 2014](#). Farinotti et al. (2019)
 195 used five models which used the ice flow dynamics to invert ice thickness from surface
 196 features to estimate the ice thickness distribution of about 21500 glaciers outside the
 197 Greenland and Antarctic ice sheets. We used the estimated data for the initial thickness
 198 distribution of Glacier1 and Glacier2 (data downloaded from
 199 <https://doi.org/10.3929/ethz-b-000315707>).

200 The Couple Model Intercomparison Project phase 6 (CMIP6) is widely used to

201 predict future climate. Eight general circulation models (GCMs) (Table 1) under two
 202 climate scenarios (SSP2-4.5 and SSP5-8.5) are used for predicting future climate. [The](#)
 203 [selected models have been well validated at the nearby catchments \(Xing et al., 2023;](#)
 204 [Yin et al., 2021; Ma et al., 2022; Zhu and Yang, 2020; Chen et al., 2022\).](#) SSP2-4.5
 205 scenario represents medium part of the future pathways, which is usually a referenced
 206 experiment comparing others CMIP6-Endorsed MIPs and it produces a radiative
 207 forcing of 4.5 W m⁻² in 2100. SSP5-8.5 scenario represents the high emission scenario
 208 and it produce a radiative forcing of 8.5 W m⁻² in 2100.

209 [There](#) [Although the reliability of GCMs has been verified in the previous studies,](#)
 210 [there](#) is certain bias in the output ~~of GCMs~~ that needs to be corrected. Firstly, outputs
 211 from eight GCMs under two climate scenarios are interpolated to 0.5°×0.5°, then the
 212 bias corrects are carried out by CMhyd software (download from
 213 <https://swat.tamu.edu/software/cmhyd/>) in which four methods were used including:
 214 distribution mapping of precipitation and temperature, linear scaling of precipitation
 215 and temperature, variance scaling of temperature and local intensity scaling (LOCI) of
 216 precipitation (Teutschbein and Seibert, 2012). The bias-corrected precipitation and
 217 temperature were calculated by using the equal weighted average method to obtain the
 218 multi-model ensemble average values under the SSP2-4.5 and SSP5-8.5 scenarios,
 219 which reduce the uncertainty caused by a single bias correction method and a single
 220 GCM, [the method is described as follow:](#)

$$P_{ave} = \frac{1}{N_{GCM}} \left(\sum_{j=1}^{N_{GCM}} \left(\frac{1}{N_{bias}} \left(\sum_{i=1}^{N_{bias}} (P_i) \right) \right) \right) \quad (1)$$

222 [Where the \$P_{ave}\$ is the average value of the multi-model and multi -method, \$P_i\$ is the](#)
 223 [projected climate data of an GCM, \$N_{bias}\$ is the number of correction methods \(\$N_{bias}\$ is 3](#)

224 [in this research](#)) and N_{GCM} is the number of GCM (N_{GCM} is 8 in this research).

225 Table 1. Details of data from eight GCMs used in this study

GCM	Institutions	Grid	Lon. × Lat.
ACCESS-CM2	Australian Community Climate and Earth System Simulator	192×144	1.875°×1.250°
ACCESS-ESM1-5	Australian Community Climate and Earth System Simulator	192×144	1.875°×1.250°
BCC-ECM1	Beijing climate center	320×160	1.125°×1.125°
CMCC-CM2-SR5	Fondazione Centro Euro-Mediterraneo sui Cambiamenti Climatici	288×192	1.25°×0.938°
CMCC-ESM2	Fondazione Centro Euro-Mediterraneo sui Cambiamenti Climatici,	288×192	1.25°×0.938°
GFDL-CM4	National Oceanic and Atmospheric Administration	144×90	2.5°×2°
MPI-ESM1-2-LR	Max Planck Institute for Meteorology	192×96	1.875°×1.875°
NESM3	Nanjing University of Information Science and Technology	192×96	1.875°×1.875°

226 3.Methodology

227 3.1 FLEX-Cryo model

228 [The FLEX-Cryo model is a landscape-based cryospheric hydrological model, that](#)
229 [which considers multiple elements multi-elements of cryosphere and their impacts on](#)
230 [hydrology, including glacier, snow and frozen soil. Figure 3 shows the structure of the](#)
231 [FLEX-Cryo model.](#)

232 [The model parameters used in this research were obtained the optimal parameter](#)
233 [set from a previous study conducted in the same catchment \(Gao et al., 2022\). The](#)

234 ~~finally~~ selected parameters are listed in Table 2 and the other variables in calculating
 235 (Fig. 3) are listed in Table 4.

236 Table 2. Model parameters and their values in this study

<u>Parameter</u>	<u>Name</u>	<u>Parameter value</u>
<u>F_{dd} ($\text{mm}^\circ\text{C}^{-1}\text{d}^{-1}$)</u>	<u>Snow degree day factor</u>	<u>3.10</u>
<u>C_g (-)</u>	<u>Glacier degree factor multiplier</u>	<u>2.27</u>
<u>S_{umax_V} (mm)</u>	<u>Root zone storage in vegetation hillslope</u>	<u>100.32</u>
<u>S_{umax_D} (mm)</u>	<u>Root zone storage in alpine desert</u>	<u>20.63</u>
<u>S_{umax_R} (mm)</u>	<u>Root zone storage in riparian wetland</u>	<u>20.26</u>
<u>β (-)</u>	<u>The shape of storage capacity curve</u>	<u>0.11</u>
<u>C_e (-)</u>	<u>Soil moisture threshold for reduction of evaporation</u>	<u>0.50</u>
<u>D (-)</u>	<u>Splitter to fast and slow response reservoirs</u>	<u>0.20</u>
<u>T_{lagf} (days)</u>	<u>Lag time from rainfall to peak flow</u>	<u>2.00</u>
<u>K_f (days)</u>	<u>Fast recession coefficient</u>	<u>1.65</u>
<u>K_s (days)</u>	<u>Slow recession coefficient</u>	<u>79.09</u>
<u>k (W (m K)^{-1})</u>	<u>Thermal conductivity</u>	<u>2.00</u>
<u>ω (-)</u>	<u>Water content as a decimal fraction of the dry soil weight</u>	<u>0.12</u>
<u>ρ (kg/m^3)</u>	<u>Bulk density of the soil</u>	<u>1000</u>
<u>P_{calt} (%/100m)</u>	<u>Precipitation increasing rate</u>	<u>4.20</u>
<u>T_{calt} ($^\circ\text{C}/100\text{m}$)</u>	<u>Temperature lapse rate</u>	<u>0.68</u>

237 3.1.1 Glacier and snow melting

238 The T_{th} threshold temperature (T_{t}) determines the phase of precipitation, i.e.
 239 snowfall or rainfall. Snow reservoir (S_w) accounts for the snow accumulating, melting
 240 (M_w) and water balance (Eq. 9). The number of days when S_w is non-zero represent the
 241 snow cover days and the maximum S_w is the maximum snow water equivalent of a year
 242 (Giovando, J. and Niemann, J. D., 2022). Both Glacier and snow melt were calculated

243 by the temperature index method, which is on basis of the degree-day factor (F_{dd}). If
244 there is no snow cover, the glacier starts to melt. Due to the lower albedo, the degree-
245 day factor of ice is greater than that of snow cover, and is multiplied by a coefficient C_g
246 to calculate glacier melt (Eq. 14).

247 3.1.2 Rainfall-runoff module

248 The rainfall and snow melt enter the root zone reservoir S_u , then runoff (R_U)
249 generates based on the input water and the relative root zone soil moisture (S_u/S_{umax})
250 and the shape of root zone storage capacity distribution determined by parameter β (Eq.
251 16). Actual evaporation E_a is also estimated based on the soil moisture S_u/S_{umax} and the
252 potential evaporation by Hamon equation (Hamon, 1961). The generated runoff (R_U) is
253 separated, by parameter D , into two linear reservoirs, i.e. the fast response reservoir (S_f)
254 and slow response reservoir (S_s) (Eq. 18 and 19). The two reservoirs are respectively
255 controlled by fast recession parameter K_f and slow recession parameter K_s to simulate
256 the subsurface storm flow Q_f and groundwater runoff Q_s (Eq. 7,8).

257 Different landscapes, for example, alpine desert, vegetation hillslope and riparian
258 zone, have different sizes of root zone storage capacity (S_{umax}) (Aubry-Wake et al.,
259 2023). In the vegetation hillslope, plants have well-developed root systems and the root
260 zone has a larger storage capacity. So Therefore, the S_{umax_V} was set to with a larger value.
261 For the alpine desert and riparian zone, the S_{umax_D} and S_{umax_R} were both limited due to
262 the less developed root system and storage capacity.

263 ~~(Gao et al., The Ah parameterization method was employed, which relies on~~
264 ~~empirical curves that are dependent on the size of the glacier.~~ 3.2 Frozen soil
265 module

266 The Stefan equation was employed to estimate freeze (thaw) depth. This equation

267 is calculated by the freeze (thaw) index (F), which neglects the sensible heat. The
268 equation is as follows:

$$269 \quad \varepsilon = \left(\frac{2 \cdot 86400 \cdot k \cdot F}{L \cdot \omega \cdot \rho} \right)^{0.5} \quad (2)$$

270 ~~w~~Where, the ε is the freeze / thaw depth (m), k is the thermal conductivity (2 W
271 (m K)⁻¹), F is the freeze/ thaw index(°C), Q_L is the volumetric latent heat of soil (J m⁻³),
272 L is the latent heat of the fusion of ice (3.35×10^5 J kg⁻¹), ω is the water content as
273 a decimal fraction of the dry soil weight (0.12), and ρ is the bulk density of the soil
274 (1000 kg m⁻³).

275 Since the Stefan equation requires ground surface temperature, which is difficult
276 to measure and often lacks data. During freezing, the air temperature was translated into
277 ground temperature by multiplier 0.6 and the ground temperature was the same as the
278 air temperature during thawing (Gisnås et al., 2016). In this research, the freeze-thaw
279 process was simulated at each Hydrologic Response Unit (RHU) by the Stefan equation
280 driven by distributed air temperature. The lower limit of permafrost was also estimated
281 by the distributed soil freeze index and thaw index where the freeze index is equal to
282 the thaw index in the mountain region.

283 In the freezing and frozen season, there is no runoff generated due to precipitation
284 in the form of precipitation being snowfall and the soil being frozen. During In this
285 period, runoff only comes from the groundwater of the supra-permafrost and no runoff
286 (R_U) is generated from root zone reservoir to the fast response reservoir (S_f) and slow
287 response reservoir (S_s). So Therefore, we set the R_U is zero in this season. In the freezing
288 season, when the freezing depth is less than 3 m, the groundwater discharge in the
289 supra-permafrost was is still connected, which could can be simulated with a linear
290 groundwater reservoir (S_s) and the slow recession coefficient (K_s). When the freezing

291 depth is greater than 3 m at a Hydrologic Response Unit, the groundwater ~~was~~ frozen
 292 and there ~~was~~ ~~is~~ little runoff generated from the groundwater discharge at the
 293 Hydrologic Response Unit. So, in the FLEX-Cryo model, the groundwater reservoir (S_s)
 294 was reduced to 10% of its storage to represent the groundwater being frozen (Eq. 3,4).
 295 The other 90% of the storage water was frozen in the groundwater system (Eq. 4). In
 296 the model, the soil ~~begin~~ ~~san~~ to freeze from high elevation to the lower elevation, which
 297 affects the groundwater. The groundwater reservoir freezes along the elevation,
 298 stopping the function of a series of cascade groundwater buckets, which is the key
 299 reason for discontinue recession.

300 In the thawing season, the freeze statue at the lowest elevation control~~s~~ing the
 301 hydraulic connectivity between groundwater system and soil. If the freeze depth is
 302 larger than thaw depth calculated by the Stefan equation, the soil is still frozen and the
 303 connectivity between groundwater system and soil is still closed. There is no runoff
 304 generated (R_u) but the ~~z~~root soil moisture (S_u) ~~is~~ ~~a~~accumulat~~e~~sing and ~~the~~ evaporation
 305 is the only outflow from the root zone. Once the thaw depth is larger than ~~the~~ freeze
 306 depth, the frozen groundwater reservoir ~~is~~ ~~was~~ released to the groundwater discharge
 307 (Eq. 4). Completely thawing at the lowest elevation represents the end of the thawing
 308 season and the start of completely thawed season. In the completely ~~thawed~~ season, the
 309 groundwater and soil are connected ~~and~~ ~~which~~ ~~is~~ not affected by the frozen soil.

310
$$\frac{dS_s}{dt} = R_s - Q_s - F_s \quad (3)$$

311
$$F_s = \begin{cases} 0.9 \cdot S_s & \text{freeze depth } (\varepsilon) \geq 3 \text{ m} \\ -0.9 \cdot S_s & \text{once thaw depth reach to yearly max} \\ & \text{or thaw depth } \geq \text{thaw depth} \end{cases} \quad (4)$$

312 **3.3 Δh -parameterization**

313 The Δh -parameterization is a mass conservation method to assess the change of

314 ice-covered, glacier length and glacier thickness in response to global warming. The
 315 glacier mass balance (GMB) calculated by FLEX-Cryo was redistributed to glacier
 316 elevation bands. It is an observed truth that the lower elevation bands loss more ice than
 317 higher elevation bands. The lost ice volume, calculated by a mass balance model, is
 318 converted into a distributed ice thickness change according to the Δh -parameterization.
 319 (Gao et al., 2021; Huss et al., 2010).

320 The Δh -parameterization method was employed, which relies on empirical curves
 321 that are dependent on the size of the glacier. The study categorized glaciers into three
 322 size classes: large valley glacier (area > 20 km²), medium valley glaciers (5 km² < area
 323 < 20 km²), and small glaciers (area < 5 km²). Both Glacier1 and Glacier2 had areas less
 324 than 5 km², and categorized as small glaciers. The small glacier equation in this study
 325 is as follows:

$$\Delta h = (h_r - 0.30)^2 + 0.60(h_r - 0.30) + 0.09 \quad (5)$$

327 Where, Δh is normalized surface elevation change and h_r is the normalized
 328 elevation range. Based on this equation, the glacier elevation and surface area were
 329 evolved every 5 years to avoid the circumstance of glacier advancing. The
 330 corresponding glacier melting HRU was transformed into alpine desert (Wei et al.,
 331 2023).

332

333 Table 3. The FLEX-Cryo model equations

<u>Landscape</u>	<u>Runoff equation</u>	<u>Water balance equation</u>	<u>Structural equation</u>
------------------	------------------------	-------------------------------	----------------------------

<u>Glacier</u>	$Q_g = \frac{S_g}{K_{f,g}} \text{ (6)}$	$\frac{dS_g}{dt} = P_l + M_g - Q_g \text{ (9)}$	$M_g = \begin{cases} F_{dd} \cdot T \cdot C_g & S_w \text{ and } T > 0 \\ 0 & S_w \text{ and } T > 0 \end{cases} \text{ (14)}$
<u>Alpine desert</u>		$\frac{dS_w}{dt} = P - M_w \text{ (10)}$	$M_w = \begin{cases} F_{dd} \cdot T & T > 0 \\ 0 & T > 0 \end{cases} \text{ (15)}$
<u>Hillslope vegetation</u>	$Q_f = \frac{S_f}{K_f} \text{ (7)}$	$\frac{dS_u}{dt} = P_l + M_w - E_a - R_u \text{ (10)}$	$R_u = (P_l + M_w) \cdot \left(1 - \left(1 - \frac{S_u}{S_{u\max}}\right)^\beta\right) \text{ (16)}$
			$E_a = E_p \cdot \left(\frac{S_u}{C_e \cdot S_{u\max}}\right) \text{ (17)}$
			$R_f = R_u \cdot D \text{ (18)}$
<u>Riparian area</u>	$Q_s = \frac{S_s}{K_s} \text{ (8)}$	$\frac{dS_f}{dt} = R_f - Q_f \text{ (12)}$	$R_s = R_u \cdot (1 - D) \text{ (19)}$
		$\frac{dS_s}{dt} = R_s - Q_s \text{ (13)}$	$R_{ft}(t) = \sum_{i=1}^{T_{lagf}} cf(i) \cdot R_f(t - i + 1) \text{ (20)}$
			$cf(i) = i / \sum_{u=1}^{T_{lagf}} u \text{ (21)}$

334 3.4 Spatial discretization of the catchment

335 The catchment area was divided into 37 elevation bands ranging from 2960 m to
336 4820 m, with an interval of 50 m. These elevation bands were classified based on four
337 landscapes: glacier, alpine desert, vegetation hillslope, and riparian zone- (Fig. 2 and
338 Fig. 3). As a result, there were a total of 148 Hydrologic Response Units (HRUs) in the
339 catchment. The landscape of alpine desert was the most widespread, covering an
340 elevation range of 3425 m to 4727 m. The glacier was found in higher altitude areas,
341 specifically between the elevation bands of 3725 m and 4727 m.

342 ~~The model parameters used in this study were obtained from a previous study~~
343 ~~conducted in this catchment (Gao et al., 2022). These parameters are listed in Table 2.~~

351 was then distributed to different elevation bands using the Δh parameterization
 352 method. Simultaneously, the glacier area and thickness were updated accordingly.
 353 When a glacier was completely melted, the corresponding HRU was transformed into
 354 alpine desert. The evolution of these landscapes was updated every 5 years (Wei et al.,
 355 2023).

356 This study focused on the degradation of glaciers, changes in snow cover and
 357 permafrost, and their impacts on runoff under climate warming. Factors such as solar
 358 radiation, land surface temperatures influenced by snow cover, and vegetation
 359 restoration were not considered. Average annual temperatures and annual precipitation
 360 were used as indicators of future climate change. Glacier thickness at the highest
 361 elevation band and glacier volume were used to quantify the thinning process of
 362 glaciers. The maximum freeze depth of seasonal permafrost, thickness of the active
 363 layer, and freeze-thaw cycle were used to characterize the thawing of frozen soil.
 364 Snow cover days and snow water equivalent were utilized to measure the decreasing
 365 trend of snow. Changes in runoff and runoff coefficient were analyzed to assess the
 366 impact of mountain cryosphere degradation on water resources. Additionally, the
 367 study examined the effect of degradation on runoff yield by observing the low runoff
 368 during the early thaw season and the discontinuation of baseflow recession.

369

370 Table 2. Model parameters and their values or ranges in this study

Parameter	Name	Prior range
F_{dd} ($\text{mm}^\circ\text{C}^{-1}\text{d}^{-1}$)	Snow degree-day factor	(1.0-5.0)
C_g (-)	Glacier degree factor multiplier	(1.0-3.0)
$S_{U_{\max_v}}$ (mm)	Root zone storage in vegetation hillslope	(50-200)

$S_{U_{max_D}}$ (mm)	Root zone storage in alpine desert	(10-100)
$S_{U_{max_R}}$ (mm)	Root zone storage in riparian wetland	(10-100)
β (-)	The shape of storage capacity curve	(0-1)
C_e (-)	Soil moisture threshold for reduction of evaporation	(0.1-0.6)
D (-)	Splitter to fast and slow response reservoirs	0.2
T_{lagf} (days)	Lag time from rainfall to peak flow	(0.8-3)
K_f (days)	Fast recession coefficient	(1-10)
K_s (days)	Slow recession coefficient	(10-100)
k (W ($m\ K$) ⁻¹)	Thermal conductivity	2
ω (-)	Water content as a decimal fraction of the dry soil weight	0.12
ρ (kg/m^3)	Bulk density of the soil	1000
P_{ealt}	Precipitation increasing rate	4.2
T_{ealt}	Temperature lapse rate	0.68

371 ~~3.1 FLEX-Cryo model~~

372 ~~FLEX-Cryo model is a landscape-based cryospheric hydrological model, which~~
373 ~~considers multi-elements of cryosphere and their impacts on hydrology, including~~
374 ~~glacier, snow and frozen soil. The elevation is also an important factor affecting the~~
375 ~~temperature and precipitation. The temperature and precipitation are interpolated~~
376 ~~based on the band in situ observation (2980 m). the temperature regression rate is~~
377 ~~0.68°C/100m and the precipitation increasing rate is 4.2%/100m. The value of 0 °C is~~
378 ~~the threshold temperature to split snowfall (P_s) and rainfall (P_r).~~

379 ~~3.1.1 Glacier and snow module~~

380 ~~Glacier and snow melt were both calculated by the temperature-index method~~
381 ~~which is on basis of the degree-day factor F_{dd} ($mm\ ^\circ C^{-1}\ d^{-1}$) (F_{dd} in Table 2; equation~~

382 (11) in Table 3). Due to the lower albedo, the degree-day of ice is greater than snow,
383 and multiplied by a coefficient C_g (C_g in Table 2; equation (9) in Table 3). The glacier
384 area runoff Q_g is calculated through the linear reservoir S_g which the liquid rain P_l and
385 glacier melt M_g inflow and the runoff outflow ((Equation (4) in Table 3) and a
386 recession parameter K_{fg} (Equation (1) in Table 3).

387 **3.1.2 Frozen soil module**

388 The Stefan equation was calculated at the different elevation bands based on the
389 interpolated temperature (Equation (18) in Table 3). The observed temperature was
390 multiplied by 0.6 to translate the air temperature to ground temperature which was
391 required in the equation. In this equation, the c is the freeze / thaw depth (m), k is the
392 thermal conductivity (2 W (m K)^{-1}), F is the freeze / thaw index ($^{\circ}\text{C}$) which represents
393 the cumulative value of the temperature below (above) 0°C , Q_L is the volumetric
394 latent heat of soil (J m^{-3}), L is the latent heat of the fusion of ice ($3.35 \times 10^5 \text{ J kg}^{-1}$),
395 ω is the water content as a decimal fraction of the dry soil weight (0.12), and ρ is the
396 bulk density of the soil (1000 kg m^{-3}).

397 The frozen soil impacts on the runoff by the soil water and groundwater. In the
398 frozen season, the baseflow comes merely from the groundwater discharge at the
399 supra-permafrost layer (Q_s). In the freezing season, when the freeze depth is greater
400 than 3 m and the supra-permafrost groundwater is frozen. And due to certain amount
401 of unfrozen water in frozen soil, the volume of slow reservoir S_s (Equation (19) and
402 (20)) will be reduced to 10%. The groundwater system in seasonal frozen soil region
403 is still connected in winter. When the soil completely thaws at the lowest elevation
404 band, the runoff generated by the frozen S_s will rapidly release to the Q_s . The
405 baseflow generation is assumed to be a linear recession process. The generated

406 baseflow is controlled by the reservoir S_s , recession coefficient K_s , the time t and
 407 initial runoff Q_0 (Equation (21)).

408
$$\frac{dS_s}{dt} = R_s - Q_s - F_s \quad (19)$$

409
$$F_s = \begin{cases} 0.9 \cdot S_s & \varepsilon \geq 3m \\ -0.9 \cdot S_s & \text{completely thaw} \end{cases} \quad (20)$$

410
$$Q = Q_0 \cdot e^{-t/K_s} \quad (21)$$

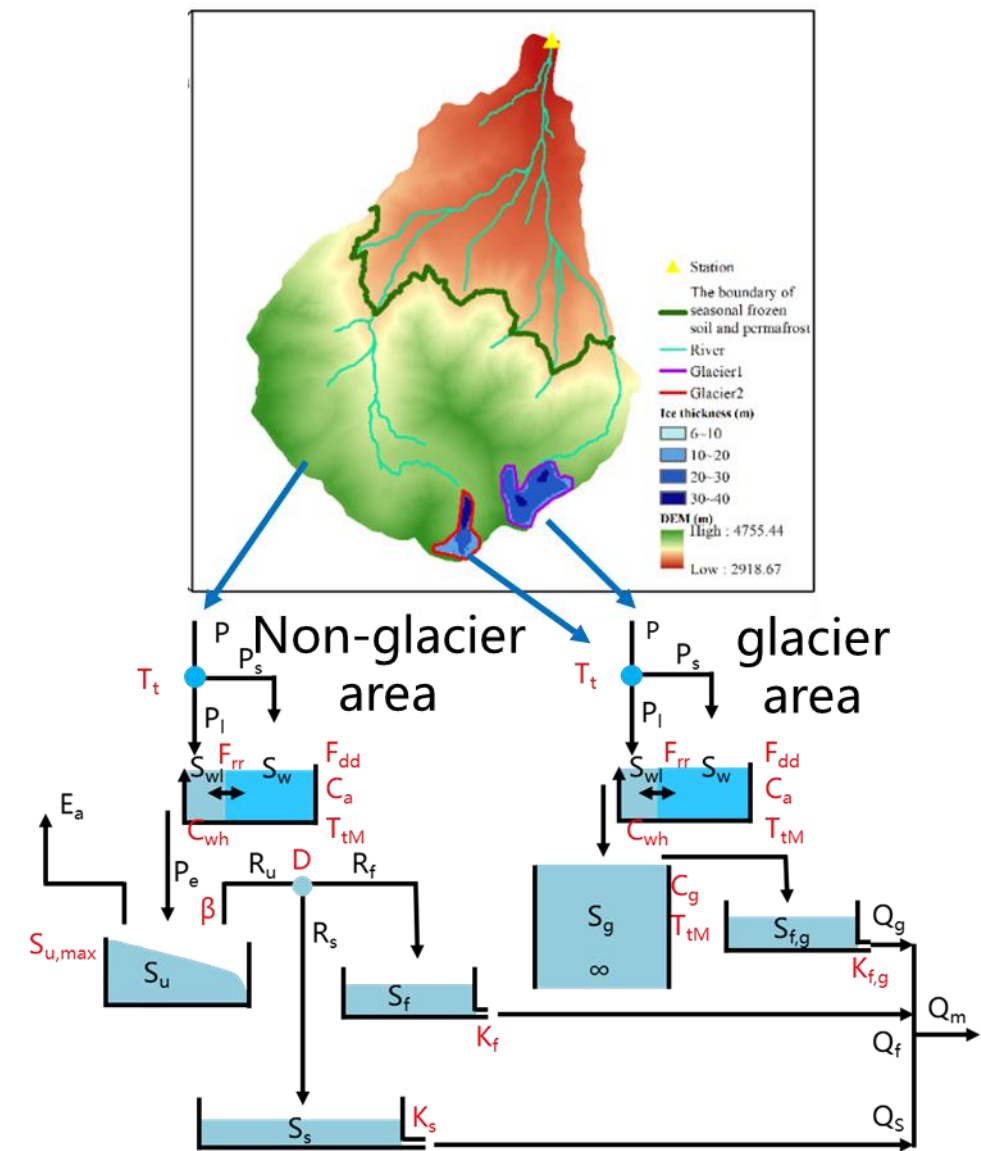
411 **3.1.3 Rainfall-runoff module**

412 The root zone reservoir S_u (equation (6) in Table 3), fast response reservoir S_f (equation
 413 (7) in Table 3) and slow reservoir S_s (equation (8) in Table 3) are critical reservoirs for
 414 simulating rainfall-runoff processes. The runoff yield process is governed by the root
 415 storage capacity and the water input to the soil (equation (12) in Table 3) meanwhile
 416 the actual evaporation is determined by soil moisture and potential evaporation. The
 417 generation runoff flows into two linear reservoirs (S_f and S_s) which represents the storm
 418 flow (Q_f) and groundwater runoff (Q_s), respectively. The runoff yield process has
 419 similarity in alpine desert, vegetation hillslope and riparian zone and the difference is
 420 the root zone storage capacity ($S_{u\max}$). In the vegetation hillslope, plants have well-
 421 developed root systems and the root zone has a larger storage capacity. So, the $S_{U\max-V}$
 422 was set with larger value. For the alpine desert and riparian zone, the $S_{U\max-D}$ and $S_{U\max-R}$
 423 were both limited due to the less developed root system and storage capacity.

424 ~~Table 3. The FLEX-Cryo model equations~~

Landscap	Runoff	Water balance equation	Structural equation
e	equation		

Glacier	$Q_g = \frac{S_g}{K_{fg}} \quad (1)$	$\frac{dS_g}{dt} = P_l + M_g - Q_g \quad (4)$	$M_g = \begin{cases} F_{dd} \cdot T \cdot C_g & S_w = 0 \text{ and } T > 0 \\ 0 & S_w > 0 \text{ and } T \leq 0 \end{cases} \quad (9)$ $\Delta h = (h_r - 0.30)^2 + 0.60(h_r - 0.30) + 0.09 \quad (10)$
Alpine desert Hillslope vegetation Riparian area	$Q_r = \frac{S_f}{K_f} \quad (2)$ $Q_s = \frac{S_s}{K_s} \quad (3)$	$\frac{dS_w}{dt} = P - M_w \quad (5)$ $\frac{dS_u}{dt} = P_l + M_w - E_a - R_u \quad (6)$ $\frac{dS_f}{dt} = R_f - Q_f \quad (7)$ $\frac{dS_s}{dt} = R_s - Q_s \quad (8)$	$M_w = \begin{cases} F_{dd} \cdot T & T > 0 \\ 0 & T \leq 0 \end{cases} \quad (11)$ $R_u = (P_l + M_w) \left(1 - \left(1 - \frac{S_u}{S_{U_{\max}}} \right)^\beta \right) \quad (12)$ $E_a = E_p \left(\frac{S_u}{C_e \cdot S_{U_{\max}}} \right) \quad (13)$ $R_f = R_u \cdot D \quad (14)$ $R_s = R_u \cdot (1 - D) \quad (15)$ $R_{ff}(t) = \sum_{i=1}^{T_{\text{logf}}} c_f(i) \cdot R_f(t - i + 1) \quad (16)$ $c_f(i) = \frac{i}{\sum_{u=1}^{T_{\text{logf}}} u} \quad (17)$ $\varepsilon = \left(\frac{2 \cdot 86400 \cdot k \cdot F}{Q_L} \right)^{0.5} - \left(\frac{2 \cdot 86400 \cdot k \cdot F}{L \cdot \omega \cdot \rho} \right)^{0.5} \quad (18)$



426

427 Figure.3 Structure of the FLEX-Cryo model. The abbreviation in red color indicates
 428 parameters and the abbreviations in black indicate storage components and fluxes.

429

[Table 4.](#) -The variables in Table 3 and [Figure 3](#) and their meaning

<u>Variables</u>	<u>Name</u> <u>Meaning</u>
<u>P (mm/day)</u>	<u>precipitation</u>
<u>T_t (°C)</u>	<u>Threshold temperature</u>
<u>P_s (mm/day)</u>	<u>Solid precipitation</u>
<u>P_l (mm/day)</u>	<u>Liquid precipitation</u>
<u>S_{wl} (mm)</u>	<u>Liquid water inside the snow pack.</u>
<u>S_w (mm)</u>	<u>Solid snow pack</u>

T_{TM} (°C)	<u>The threshold temperature for snow and glaciers melting</u>
P_e (mm)	<u>Generated runoff to soil/ice surface</u>
E_a (mm)	<u>Actual evaporation</u>
R_u (mm)	<u>water that exceeds the storage capacity</u>
S_f (mm)	<u>Fast flow reservoir</u>
S_s (mm)	<u>Slow flow reservoir</u>
$S_{f,g}$ (mm)	<u>Glacier linear reservoir</u>
Q_f (mm/day)	<u>Subsurface storm flow</u>
Q_s (mm/day)	<u>Groundwater runoff</u>
Q_g (mm/day)	<u>Runoff in glacier region</u>
Q_m (mm/day)	<u>All runoff</u>

3.5 Model evaluation metrics

The Kling–Gupta efficiency (KGE), Nash–Sutcliffe efficiency (NSE), coefficient of correlation (R) and root mean square error (RMSE) were used to comprehensively assess ~~assessment of the~~ model performance and ~~it also indicates~~ the reliability for the model. All The KGE, NSE, R and RMSE are all less than 1. For KGE, NSE and R, values closer to 1 indicate ~~The first three valuation closer 1 indicates the better~~ performance. ~~and the~~ A lower RMSE value indicates less error and better model performance. These metrics can be calculated as follows:

$$KGE = 1 - \sqrt{(r - 1)^2 + (\alpha - 1)^2 + (\beta - 1)^2} \quad (22)$$

$$NSE = 1 - \frac{\sum_{t=1}^n (Q_0 - Q_m)^2}{\sum_{t=1}^n (Q_0 - \bar{Q}_0)^2} \quad (23)$$

$$RMSE = \sqrt{\frac{1}{N} \sum_{i=1}^n (Q_0 - Q_m)^2} \quad (24)$$

$$R = \frac{\sum_{t=1}^n (Q_0 - \bar{Q}_0)(Q_m - \bar{Q}_m)}{\sqrt{\sum_{t=1}^n (Q_0 - \bar{Q}_0)^2} \sqrt{\sum_{t=1}^n (Q_m - \bar{Q}_m)^2}} \quad (25)$$

where, r is linear correction coefficient between simulation and observation, α

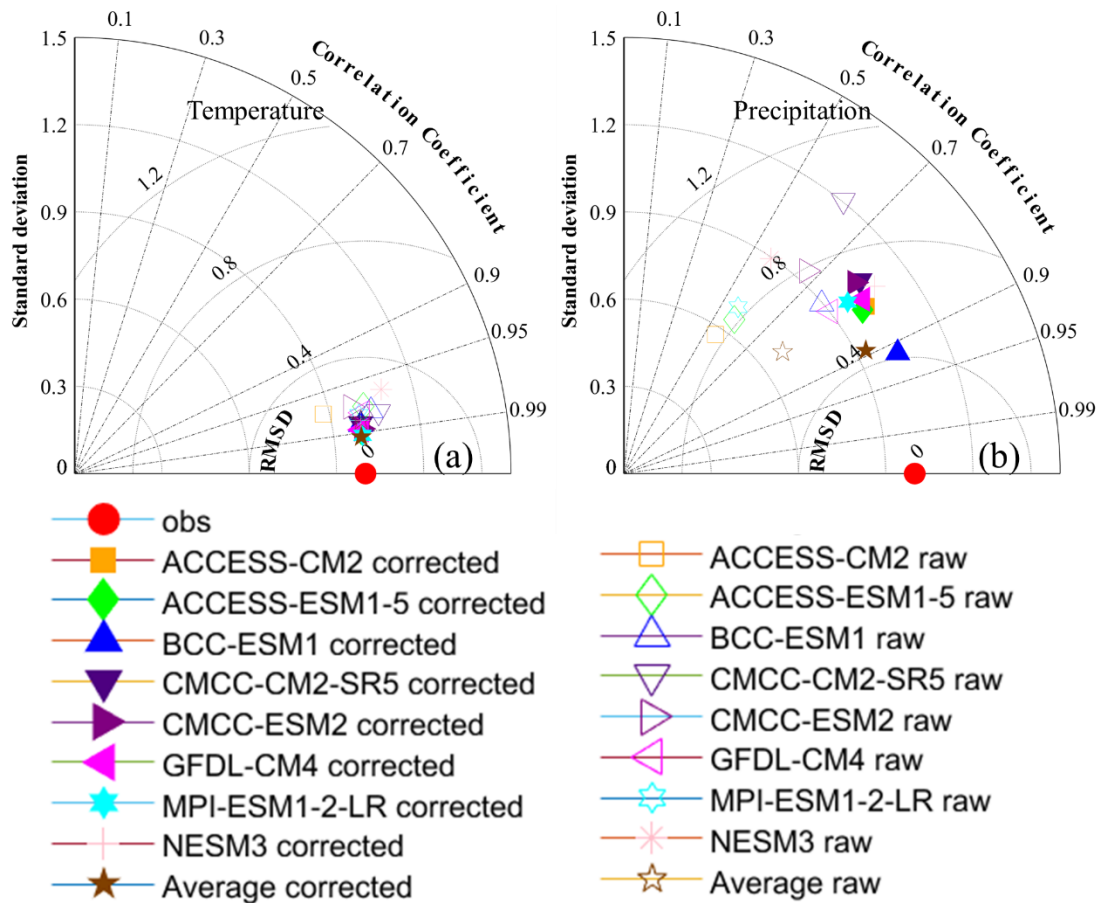
443 is the ratio of the stand deviation of simulated variables and observed variables, β is
444 the ratio of the average value of simulated and observed variables, Q_0 is the observation
445 runoff, $\overline{Q_0}$ is the average observed runoff and Q_m is the simulation runoff.

446 **4. Results**

447 **4.1.4.1 Performance of bias correction and runoff depth simulation**

448 **4.1.1 Bias correction performance**

449 The ~~precision~~accuracy of climate projection varied with the multiple bias
450 correction method (Fig. 4). The distance between the observation and the projection is
451 inversely proportional to the ~~accuracy~~precision. Before the bias correction, the distance
452 is relatively far especially for precipitation indicating that there is a large error between
453 observatio~~n~~ and GCMs projection. After the bias correction, the distance
454 diminishes~~minish~~, indicating that the bias correction improves the accuracy,
455 particularly for ~~precision~~ especially for precipitation.

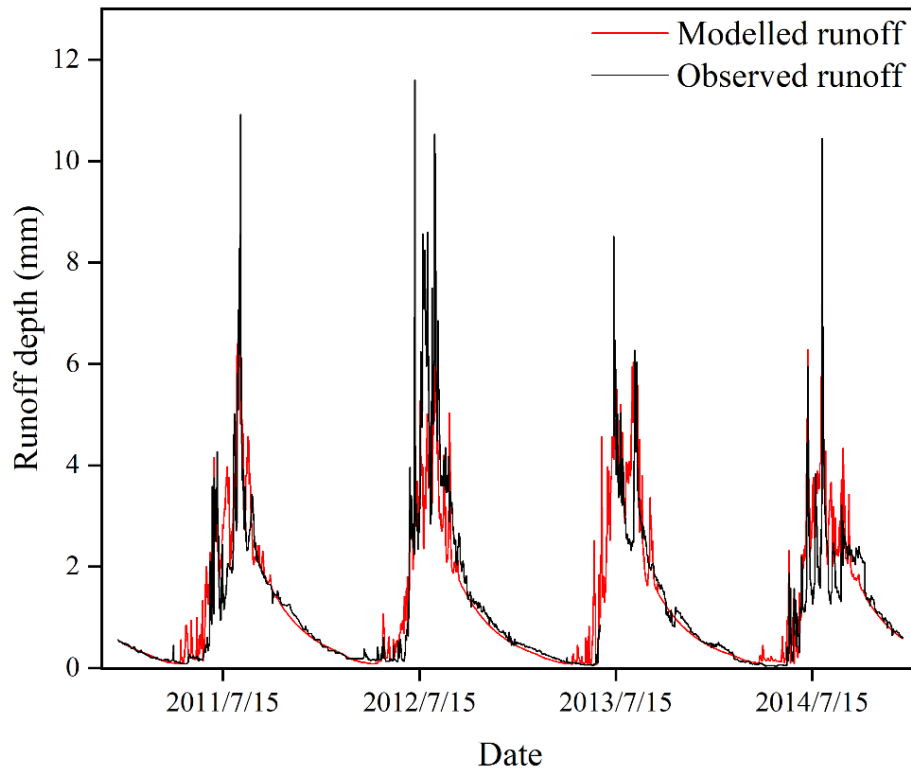


456 Figure 4. Taylor diagram of monthly temperature and precipitation simulation.

457 The hollow points are the uncorrected projection, the solid point are the corrected
 458 projection and the solid red circle is the reference values (observation).

460 4.1.2 Performance of runoff simulation

461 We assessed FLEX-Cryo the performance of the FLEX-Cryo model for runoff
 462 simulation based on historical observations. Throughout the entire assessment period,
 463 the KGE is 0.83, NSE is 0.73, R is 0.74, and RMSE is 0.77 mm/day. These results
 464 indicate that the model can reproduce hydrographs effectively. The good model
 465 performance demonstrates the robustness of the FLEX-Cryo model, ensuring accurate
 466 estimation of future hydrological changes (Fig. 5).

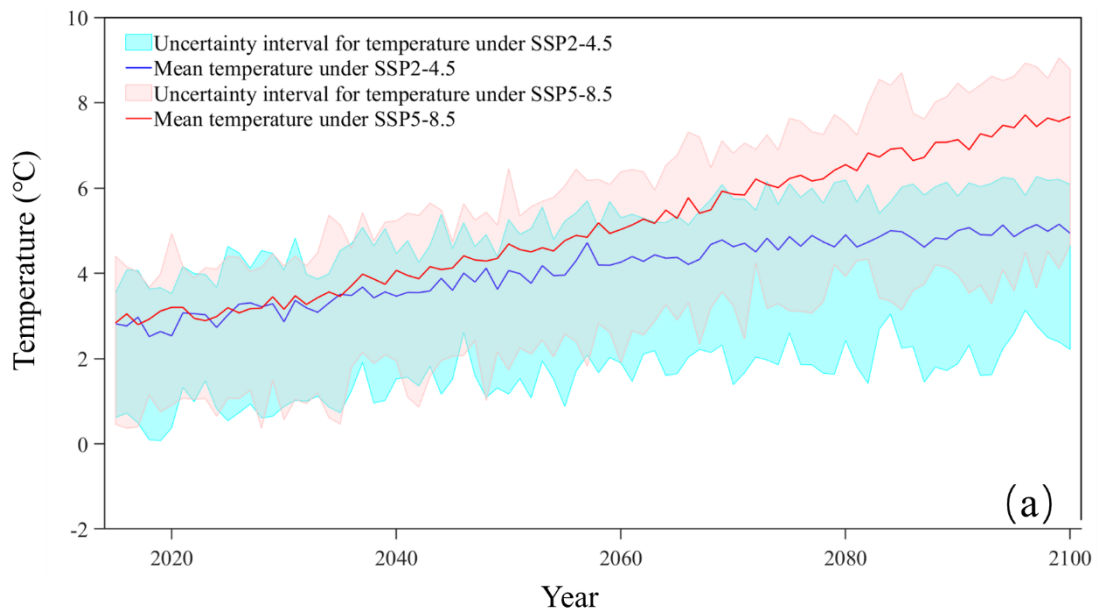
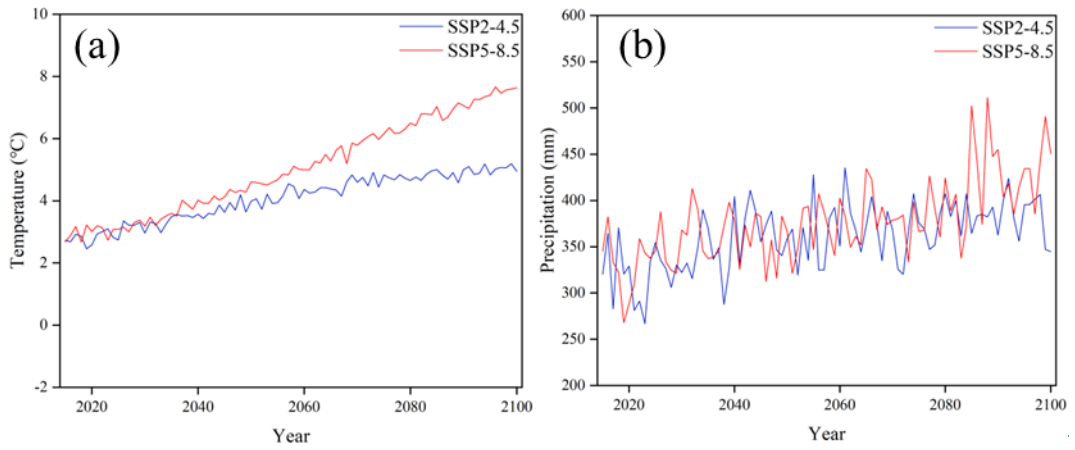


467
 468 [Figure.5 Simulation results of the FLEX-Cryo model and the comparisons with](#)
 469 [observation from 2011 to 2014.](#)

470 **[4.2 Future climate change](#)**

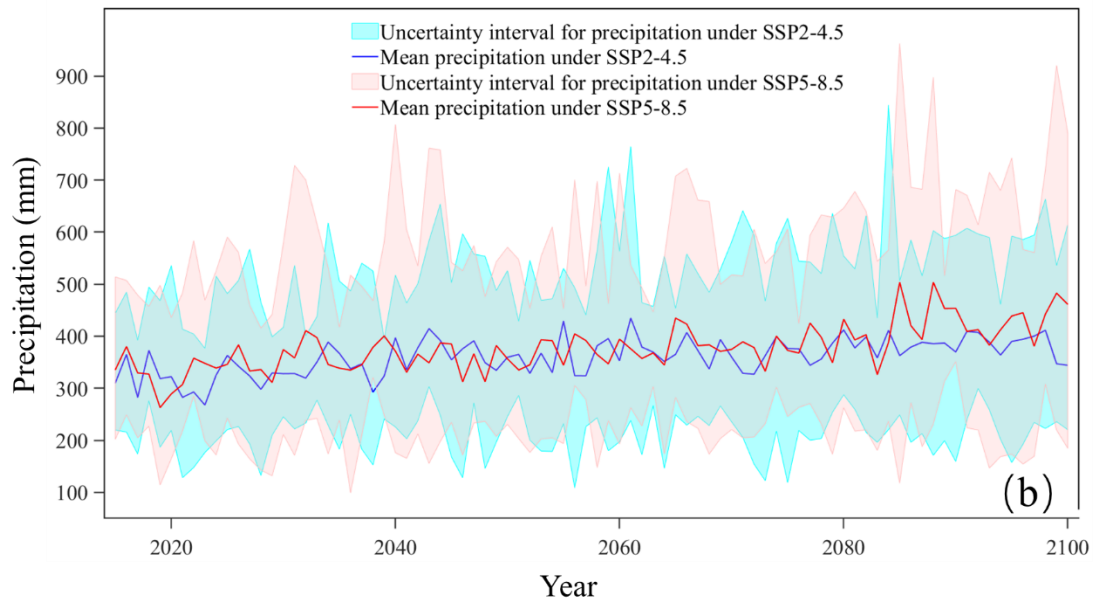
471 Figure 46 shows the prediction of future climate in 2015-2100 under the SSP2-4.5
 472 and SSP5-8.5 [scenarios](#) based on the average values of eight climate models (adjusted
 473 for bias). According to the SSP2-4.5 [scenario](#), the temperature will increase by 2.07°C
 474 relatively steadily by 2100. Under the SSP5-8.5 [scenario](#), temperatures are projected to
 475 continue to rise by 5.04°C over the course of the century. Precipitation changes are
 476 more [drastic](#) than temperature, especially after the eighties of the 21st century
 477 under the SSP5-8.5 [scenario](#). Overall, the precipitation under the SSP2-4.5 [scenario](#)
 478 increased by 14.25 %, and the precipitation increased by 33.50 % under the SSP5-8.5
 479 [scenario](#). Before the [80s of the 21st century](#) [2080s](#), the increase in precipitation was
 480 almost the same under different scenarios, about 8.9 mm 10 years⁻¹ and 8.5 mm 10

481 years⁻¹, respectively. [Although there are some uncertainties associated with temperature](#)
482 [and precipitation, the increasing trend of temperature and precipitation are still](#)
483 [distinguished, especially for the SSP5-8.5.](#)



485

486



487

488 Figure 4. The6. (a) the annual average temperature (a) and (b) annual precipitation
 489 mean (b) of bias adjusted multi-Global Climate Model from 2015-2100. The blue and
 490 red areas indicate the uncertainty caused by 8 climate change models of SSP2-4.5 and
 491 SSP 5-8.5 scenarios.

492 4.23 The change of cryosphere in the future

493 4.3.1 Predicting glacier retreat

494 In the initial status (Figure 5), the Glacier1 and Glacier2 had areas of 8.78×10^5
 495 m^2 and $4.08 \times 10^5 m^2$, and ice volumes of $20.13 \times 10^6 m^3$ and $8.86 \times 10^6 m^3$, respectively.
 496 Glacier1 exhibited greater-7 shows changes in glacier thickness at the highest
 497 elevation band and volume compared to Glacier2.

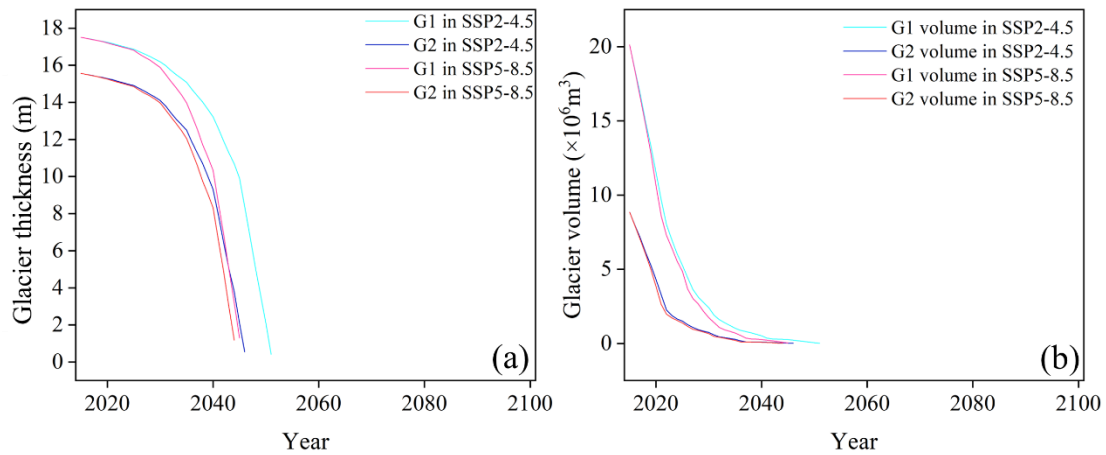
498 Both Glacier1 and Glacier2 experienced retreat, characterized by a decrease in
 499 glacier volume and thinning of glacier thickness (Figure 5).for the Glacier 1 and the
 500 Glacier 2 under two SSPs from years 2015–2100. Starting from the 2020s, the glacier
 501 volume showed a rapid decline, and after the 2030s, the highest altitude portion of the
 502 glacier entered a phase of rapid thinning. Around 2040, the glacier degradation reached

503 a stabilization period, during which glaciers were only present in the highest elevation
504 band. According to the SSP2-4.5 scenario, Glacier1 and Glacier2 are projected to
505 completely melt and disappear by 2051 and 2046, respectively. Under the SSP5-8.5
506 scenario, the complete melt-out time is slightly earlier, occurring in 2045 and 2044 for
507 Glacier1 and Glacier2, respectively. After the glaciers completely melt, ~~approximately~~
508 ~~5.6% of the~~ ablated glacier area will transform into alpine desert.

509 Taking the glacier changes in 2025, 2035, and 2045 as examples, under the SSP2-
510 4.5 scenario, the area of Glacier1 is projected to decrease to $5.49 \times 10^5 \text{ m}^2$, $1.52 \times 10^5 \text{ m}^2$,
511 and $0.26 \times 10^5 \text{ m}^2$, with corresponding volume reductions to $5.27 \times 10^6 \text{ m}^3$, $1.03 \times 10^6 \text{ m}^3$,
512 and $0.26 \times 10^6 \text{ m}^3$, respectively (~~Figure 7~~[Fig. 9](#)). Comparatively, the retreat trend is more
513 pronounced under the SSP5-8.5 scenario. The area of Glacier1 is projected to be
514 $4.00 \times 10^5 \text{ m}^2$, $0.81 \times 10^5 \text{ m}^2$, and $0.26 \times 10^5 \text{ m}^2$, with volumes of $4.86 \times 10^6 \text{ m}^3$, 0.71×10^6
515 m^3 , and $0.03 \times 10^6 \text{ m}^3$, respectively. The degradation of Glacier2 follows a similar
516 pattern to that of Glacier1, except that Glacier2 experiences less ice loss. According to
517 the SSP5-8.5 scenario, Glacier2 is projected to completely melt by 2045. In 2025 and
518 2035, the area of Glacier2 ~~remains consistent, with values of~~ $1.67 \times 10^5 \text{ m}^2$ and
519 $0.51 \times 10^5 \text{ m}^2$ for both scenarios, respectively. These glaciers are only distributed within
520 the elevation bands from 4625 m to 4727 m and from 4675 m to 4727 m.

521

522



523

524

Figure 5-7. The glacier thickness (a) and glacier volume (b) change from 2015 to

525

2100 for the Glacier1 and Glacier 2

526

4.3.2 Forecasting the degradation of frozen soil

527

~~In the initial state (Figure 6), the~~ The degradation of seasonal frozen

528

~~soil seasonally frozen soil exhibited an early freeze onset in early November, with a~~

529

~~freeze duration of approximately 200 days at the lowest elevation band. The~~ and

530

~~permafrost, on the other hand, experienced a thaw onset in mid-June, lasting around~~

531

~~120 days at the highest elevation band. The maximum freeze depth was~~

532

~~approximately 2.30 m at lower altitudes, while the active layer thickness measured~~

533

~~around 1.27 m at the highest elevation.~~

534

~~By the end of the 21st century, under the SSP2-4.5 scenario, several changes are~~

535

~~projected to occur. The~~ by FLEX-Cryo model. Under SSP2-4.5, by the end of 21st

536

~~century, the~~ freeze onset of seasonally frozen soil will be delayed

537

~~by 10 days, resulting in a shortened~~ and the freeze-thaw cycle duration ~~of~~ will shorten

538

~~approximately 1 month. The maximum freeze depth of seasonally frozen soil is~~

539

~~expected to decrease by 5.17 cm per decade.~~ The thaw onset of permafrost will be

540

~~advanced by 19 days, leading to an increased~~ and the freeze-thaw cycle duration ~~of~~

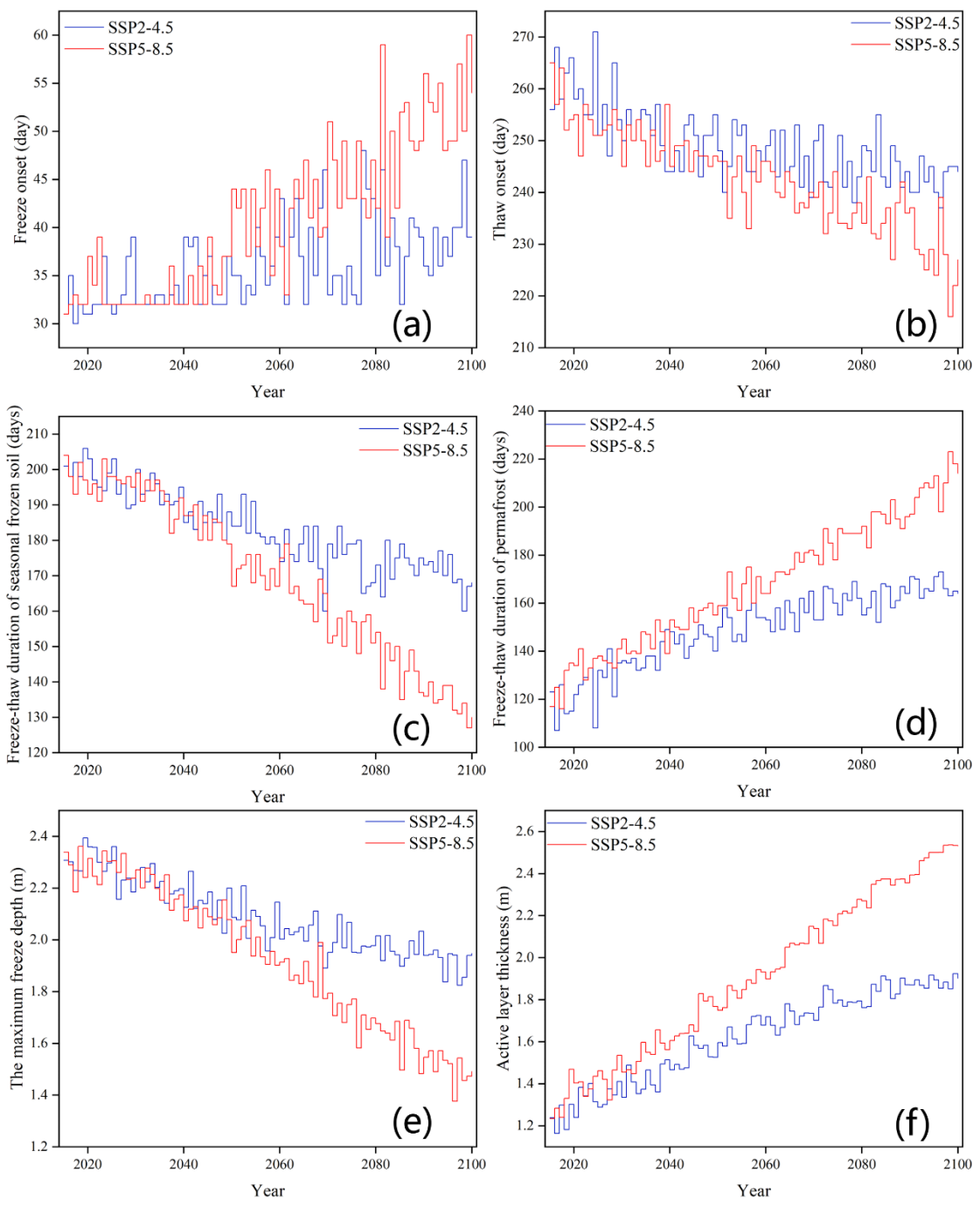
541

~~would increase~~ nearly 50 days. Additionally, the maximum freeze depth is expected to

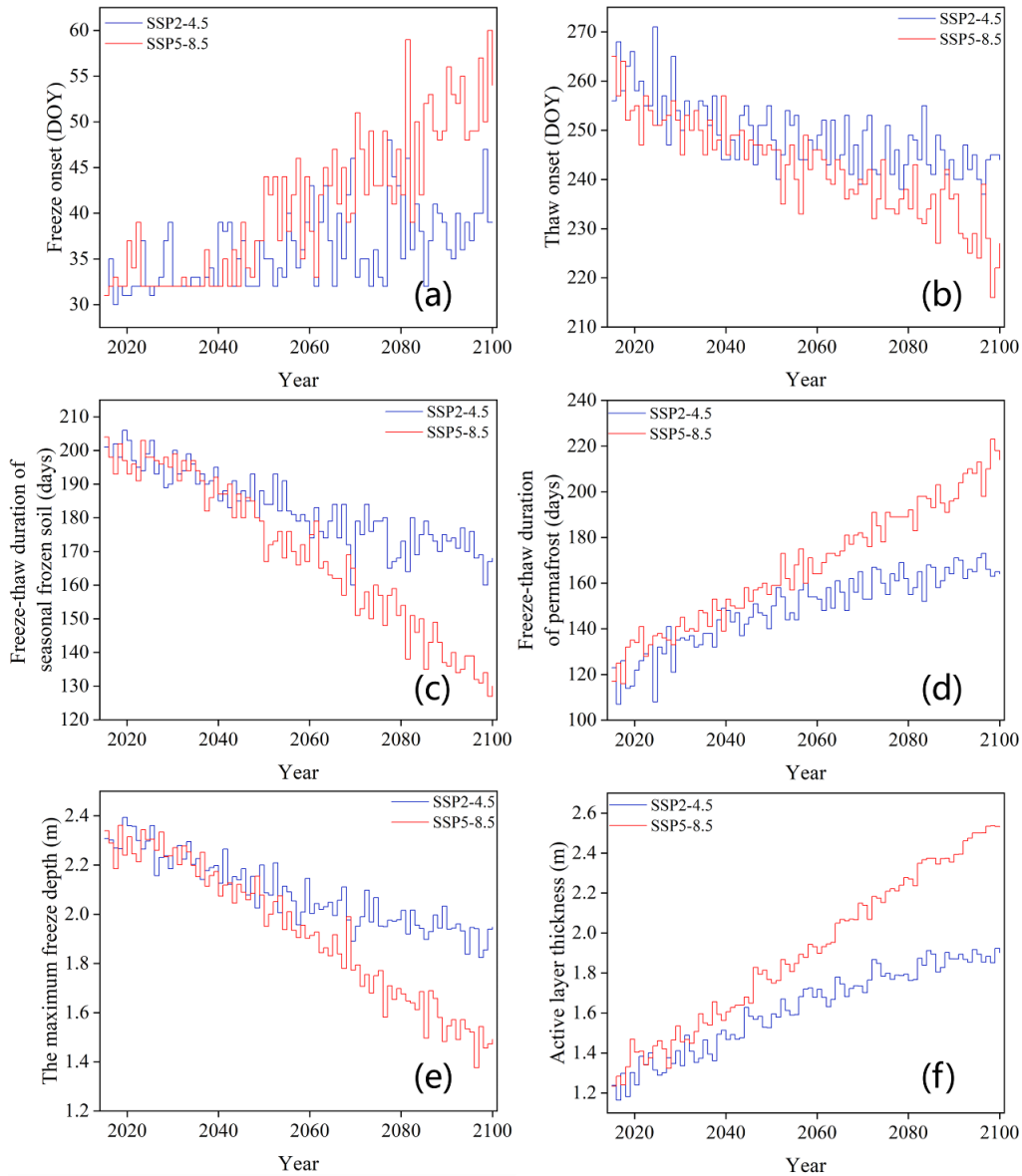
542 ~~decrease by 5.17 cm per decade, while the~~The active layer thickness will ~~increase~~rise
543 by approximately 8.24 cm per decade. ~~The~~ Meanwhile, the degradation trend of
544 permafrost is more severe under the SSP5-8.5 scenario. ~~By the end of the 21st century,~~
545 ~~compared to the~~Under SSP2-4.5 ~~scenario~~, the freeze onset of ~~seasonal frozen~~
546 ~~soil~~seasonally frozen soil will be shortened by 22 days, ~~resulting in a further reduction~~
547 ~~of and~~ the freeze-thaw cycle duration will reduce by over 2 months. The thaw onset of
548 permafrost will occur approximately 1 month earlier, and the freeze-thaw cycle duration
549 of permafrost will increase by nearly 3 months. ~~The~~Compared with the SSP2-4.5, the
550 decreasing trend of the maximum freeze depth and the increasing trend of the active
551 layer thickness are approximately twice as pronounced under the SSP5-8.5 ~~scenario~~
552 ~~compared to the SSP2-4.5 scenario. While the freeze onset of seasonal frozen soil~~
553 ~~exhibits significant variation between consecutive years, the other frozen soil elements~~
554 ~~follow a more stable change pattern. Before 2040, there is little difference between the~~
555 ~~two scenarios, except for the active layer thickness. By 2100~~ Seasonal frozen
556 ~~soil~~Seasonally frozen soil will begin to freeze around mid-November and late
557 November, while permafrost will start to thaw in mid-May and early June by the year
558 2100 under two SSPs.

559 Under the SSP2-4.5 and SSP5-8.5 ~~scenarios~~, the lower limit of permafrost
560 gradually expands along the altitudinal gradient, with rates of 4.30 m per year and 8.75
561 m per year, respectively (~~Figure 7~~Fig. 9). In the SSP2-4.5 ~~scenario~~, the lower limit of
562 permafrost is projected to reach altitudes of 3685 m, 3795 m, 3835 m, 3865 m, 3985 m,
563 and 4015 m in the years 2025, 2035, 2045, 2055, 2075, and 2095, respectively. The
564 lower limit of permafrost in 2095 under the SSP2-4.5 scenario is comparable to the
565 lower limit of permafrost (~~3965 m~~3965m) in 2055 under the SSP5-8.5 scenario. ~~Before~~

566 2045, the lower bound exhibits similar changes under both scenarios, but a significant
 567 divergence occurs afterward. The lower limit is projected to increase to 4355 m by 2095
 568 under the SSP5-8.5 scenario.



569



570

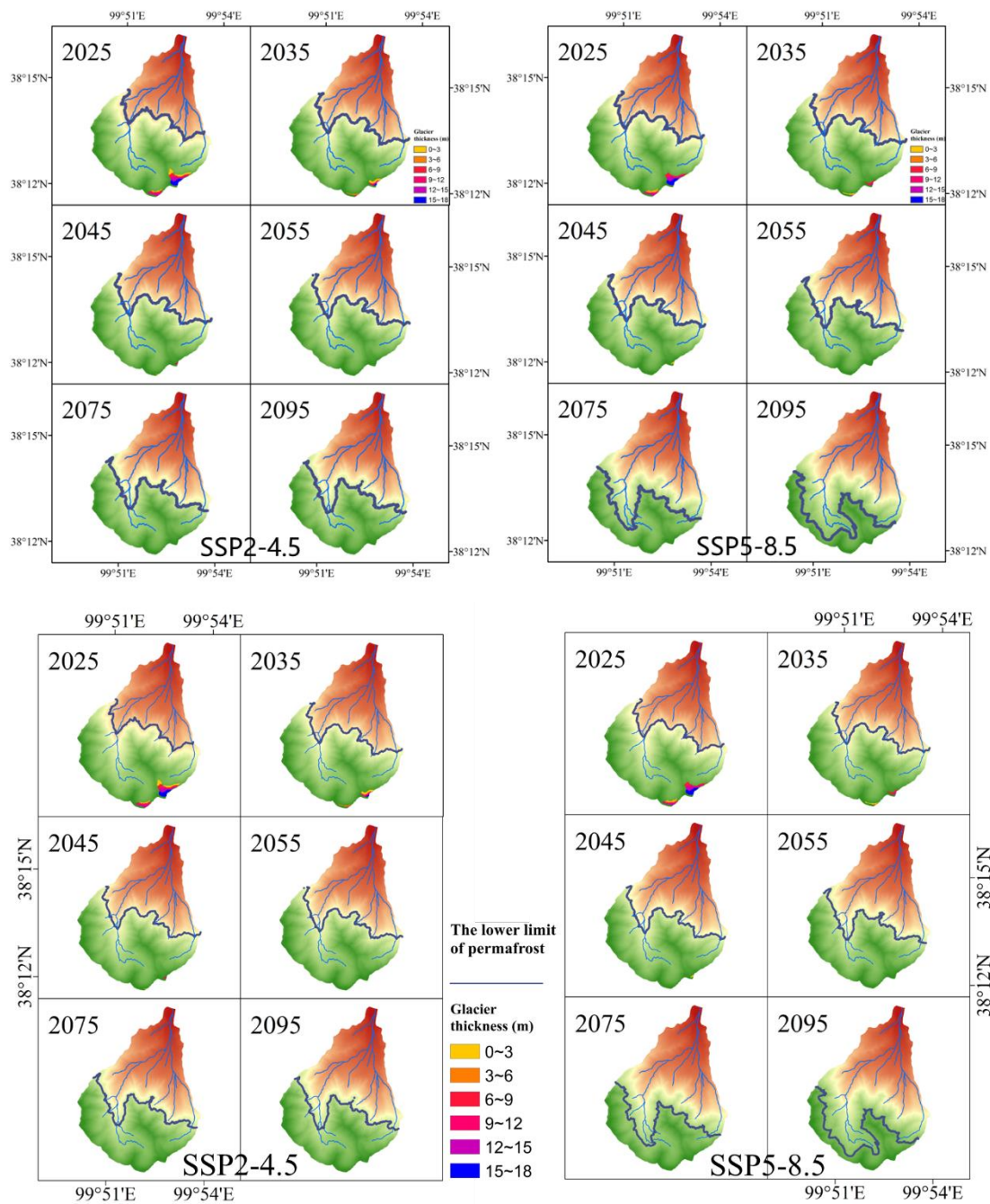
571 Figure 68. Changes in seasonally frozen soil and permafrost

572 from 2015-2100 under SSP2-4.5 and SSP5-8.5 scenarios. (a, b) Freeze and thaw onset.

573 (c, d) Freeze-Thaw duration of frozen soil and permafrost. (e, f) The maximum freezing

574 depth and active layer thickness.

575



576

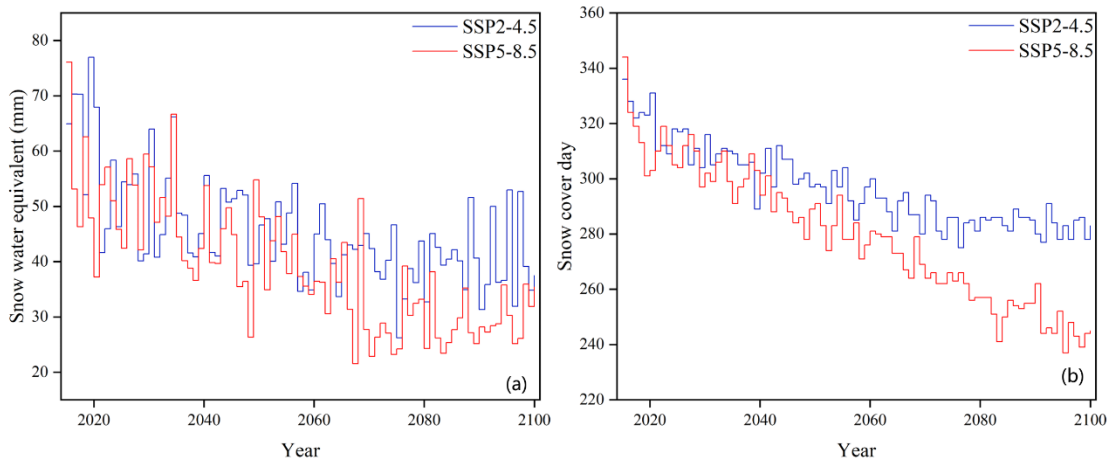
577

578 Figure 79. Changes of ice thickness and the lower limit of permafrost in 2025, 2035,
 579 2045, 2055, 2075 and 2095 under SSP2-4.5 and SSP5-8.5.

580 **4.43.3 Snow change in the future**

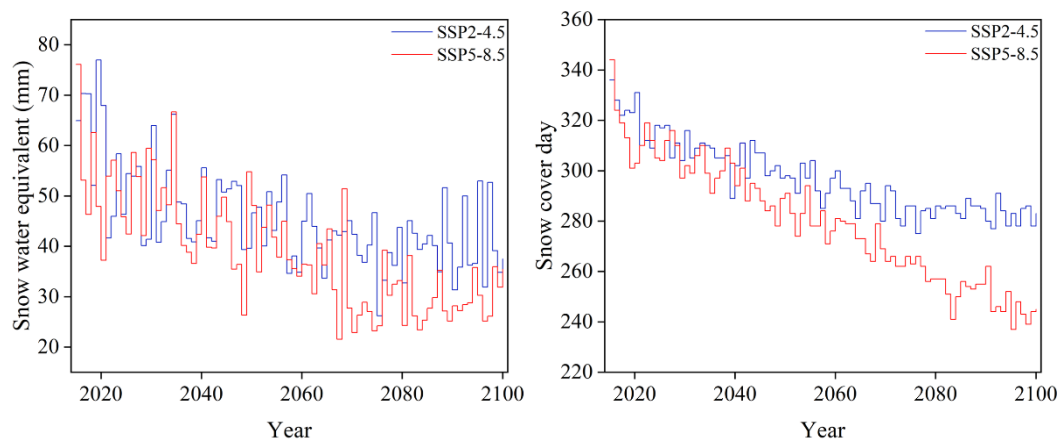
581 The duration of snow cover is projected to decrease continuously in the future-
 582 (Fig. 10). Under the SSP2-4.5-scenario, the snow cover days are likely to be
 583 shortened by 45 days, while under the more severe SSP5-8.5 scenario, the reduction is

584 expected to be around 76 days. Simultaneously, the snow water equivalent, which
 585 measures the amount of water contained in the snowpack, is projected to exhibit more
 586 variable changes but with an overall decreasing trend. For the SSP2-4.5 scenario, the
 587 and snow water equivalent will decrease by 0.24 mm per year, resulting in. Compared
 588 with SSP 2-4.5, snow cover has a more reduction of approximately 41.4%.under
 589 SSP5-8.5. Under the SSP5-8.5 scenario, the decrease in snow water equivalent is
 590 more pronounced, with a drop of 0.35 mm per year, corresponding to a reduction of
 591 up to 46.0%.



592 Figure 8. (a) snow water equivalent at entirely watershed and (b), snow cover day
 593 at the highest band, is expected to be around 76 days and snow water equivalent will
 594 decrease by 0.35 mm per year.

596 **4.5**



597

598 [Figure 10. Changes of snow water equivalent and snow cover day from 2015-2100](#)
599 [under SSP2-4.5 and SSP5-8.5.](#)

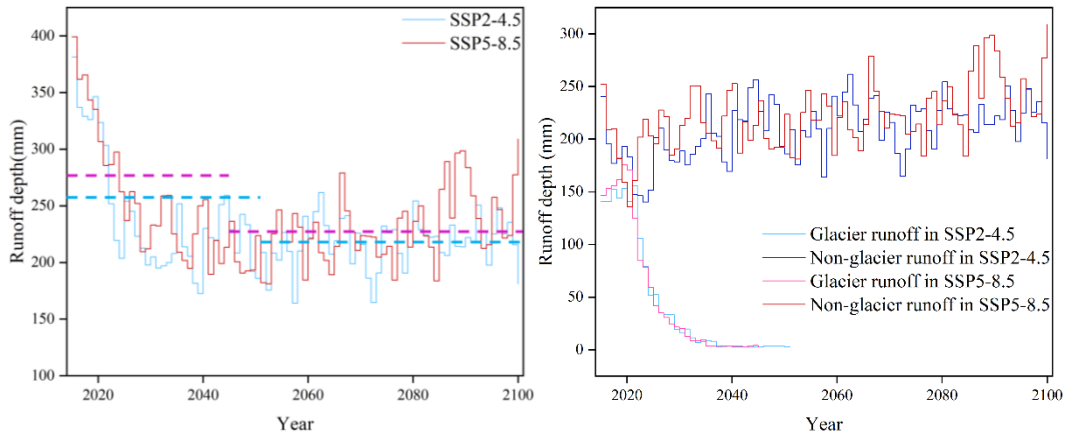
600 **[4.4 Projected future runoff](#)**

601 [The depth of runoff in the entire basin shows a declining trend in the future.](#)
602 [Under both the SSP2-4.5 and SSP5-8.5 scenarios, before the complete melting of](#)
603 [glaciers, the runoff depth is estimated to be around 257 mm and 277 mm, respectively.](#)
604 [After the glaciers completely melt, the runoff depth is projected to decrease by](#)
605 [15.56% and 18.05% for the SSP2-4.5 and SSP5-8.5 scenarios, respectively \(Figure 9\).](#)
606 [By 2100, the average annual runoff depth is expected to be similar for both scenarios,](#)
607 [at approximately 217 mm and 227 mm. In the SSP2-4.5 and SSP5-8.5 scenarios, the](#)
608 [tipping point for the runoff depth in the glacier area is projected to occur in 2021 and](#)
609 [2019, respectively, with values of 155.93 mm and 175.98 mm. After reaching the](#)
610 [tipping point, the runoff depth in the glacier area is likely to continue decreasing until](#)
611 [the glaciers completely melt. In non-glacier areas, the runoff depth shows an increase](#)
612 [of 0.48 mm per year and 0.65 mm per year.](#)

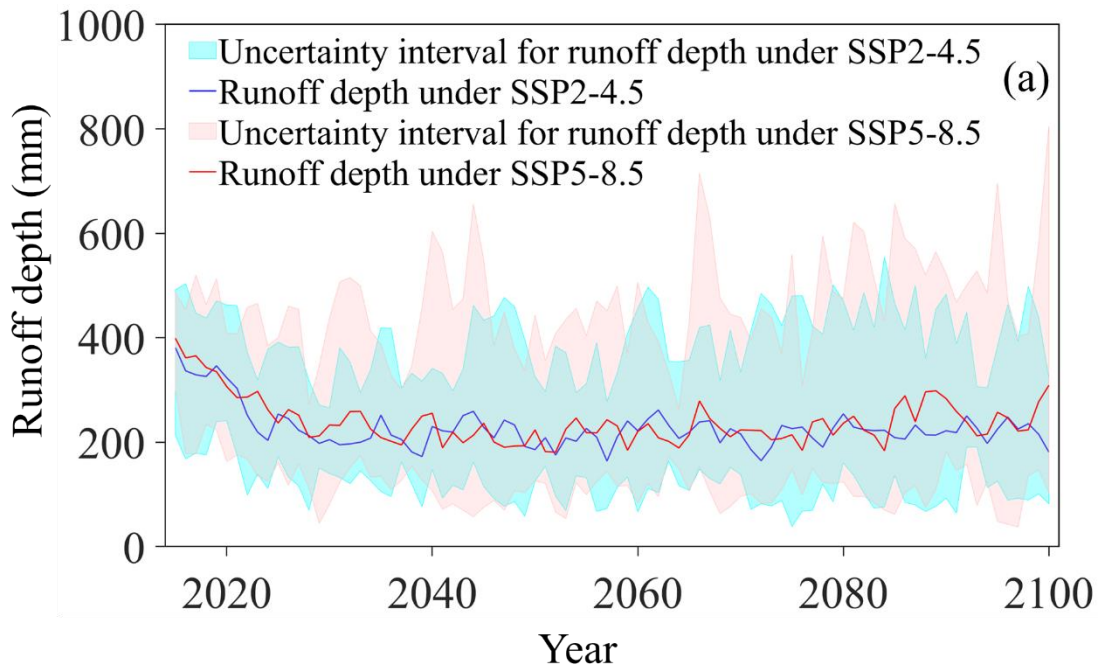
613 [The runoff in the catchment were predicted by the FLEX-Cryo model under SSP2-](#)
614 [4.5 and SSP5-8.5. The tipping point of the glacier melting has already occurred \(around](#)
615 [2020\). After the turning point, glacier runoff and runoff of the total basin decreases](#)
616 [dramatically until glacier completely melt. Then the runoff of the total basin will](#)
617 [moderate increase. After glacier completely melt, runoff of the total basin would](#)
618 [decrease by 15.56% and 18.05% respectively.](#) The runoff coefficient, which represents
619 the proportion of precipitation that becomes runoff, follows a similar pattern to the
620 glacier runoff changes. It initially increases [until the turning point of glacier melting](#)
621 [occurs](#), then decreases, and eventually reaches a relatively stable state after the glaciers

622 completely melt (~~Figure 10~~Fig. 11 (c)). Before the turning point, runoff coefficient is
623 almost equal or even greater than 1. The maximum values of the runoff coefficient occur
624 in 2021 and 2019, coinciding with the tipping points of the glacier runoff. By the end
625 of the 21st century, the runoff coefficient is projected to be dramatically reduced to
626 approximately 0.42. These results indicates that glacier play a key role in water resource
627 supply.

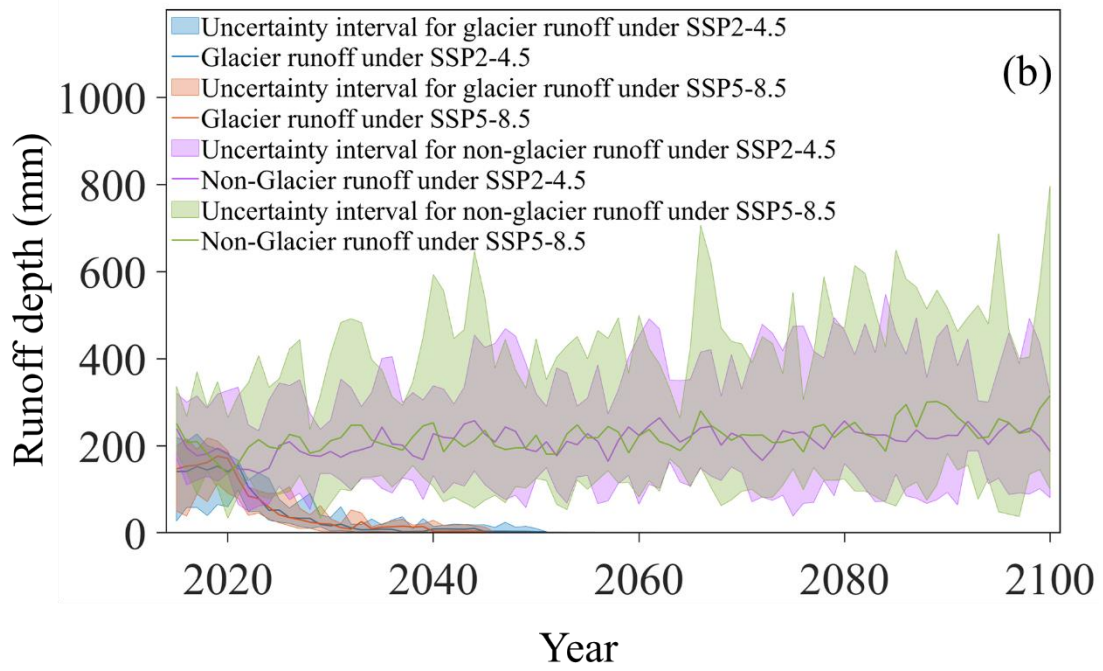
628 Two hydrological phenomena observed in permafrost mountainous catchments,
629 namely the low runoff in the early thawing season (LRET) and discontinuous baseflow
630 recession (DBR) (Gao et al., 2022), are expected to persist in the future (~~Figure 11~~Fig.
631 12). Meanwhile, baseflow, which represents the sustained flow of water from
632 groundwater, shows an increasing trend. The duration of the early thawing season is
633 projected to be further reduced. The first recession coefficient remains unchanged,
634 while the second recession coefficient progressively increases. Under the SSP2-4.5
635 scenario, the second recession coefficient is equal to 74 days, which is consistent with
636 the recession coefficient in 2060 under the SSP5-8.5 scenario. This suggests that the
637 permafrost area undergoes less significant changes under SSP2-4.5 scenario than SSP2-
638 8.5 scenario according to Figure 79. The baseflow gradually increases, especially in the
639 SSP5-8.5 scenario, as indicated by the runoff depth on a logarithmic scale (~~Figure XX~~
640 12).



641



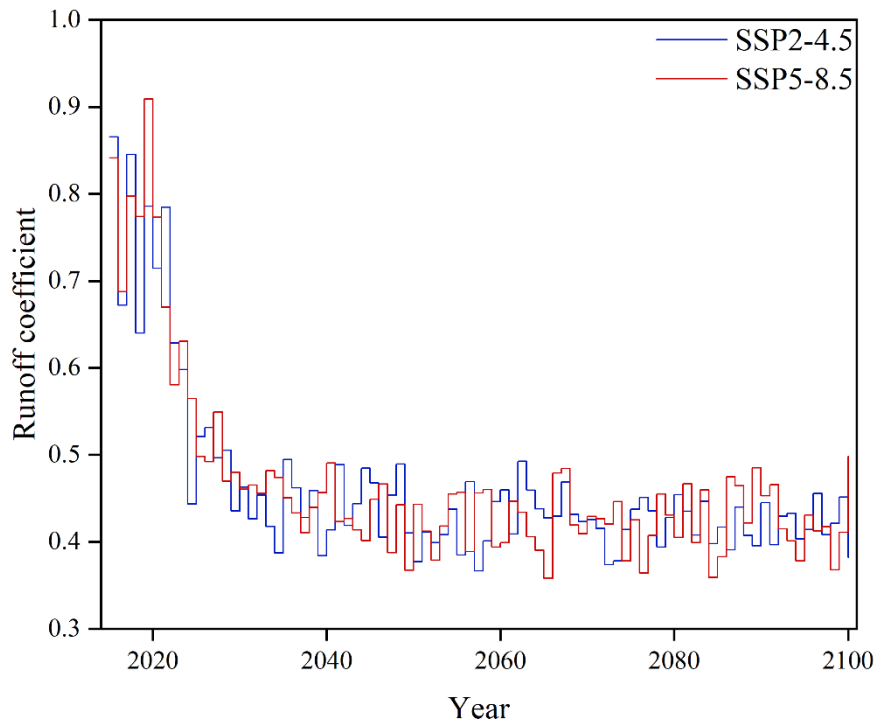
642



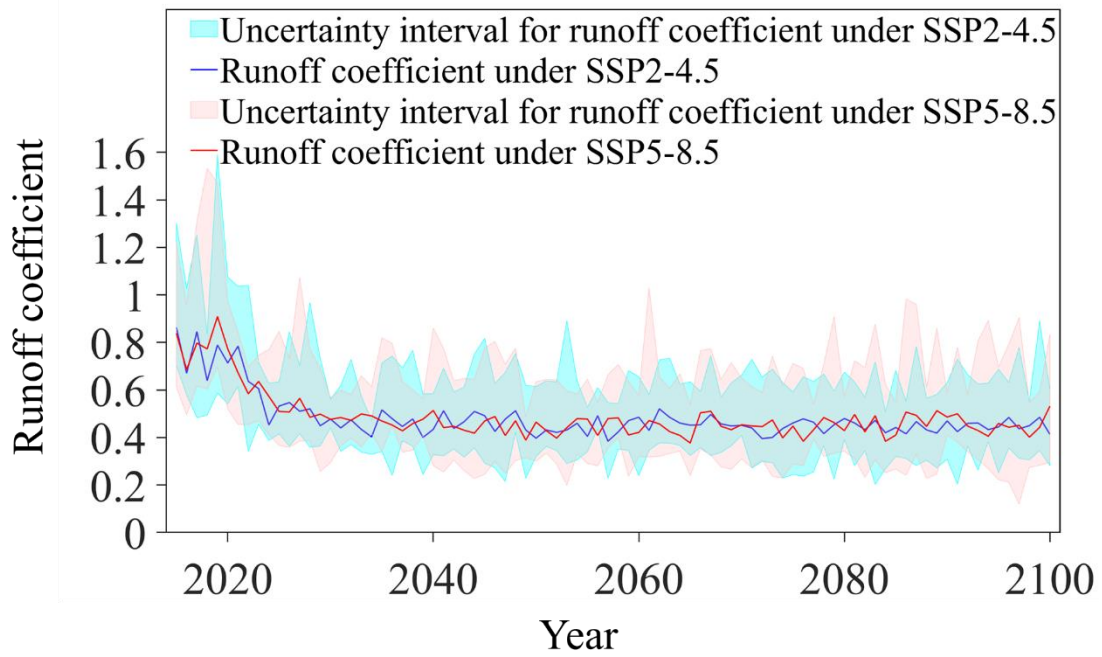
643

644 [Figure 9. \(a\) The predicted runoff depth of the total basin \(b\) Runoff in the glacier and](#)

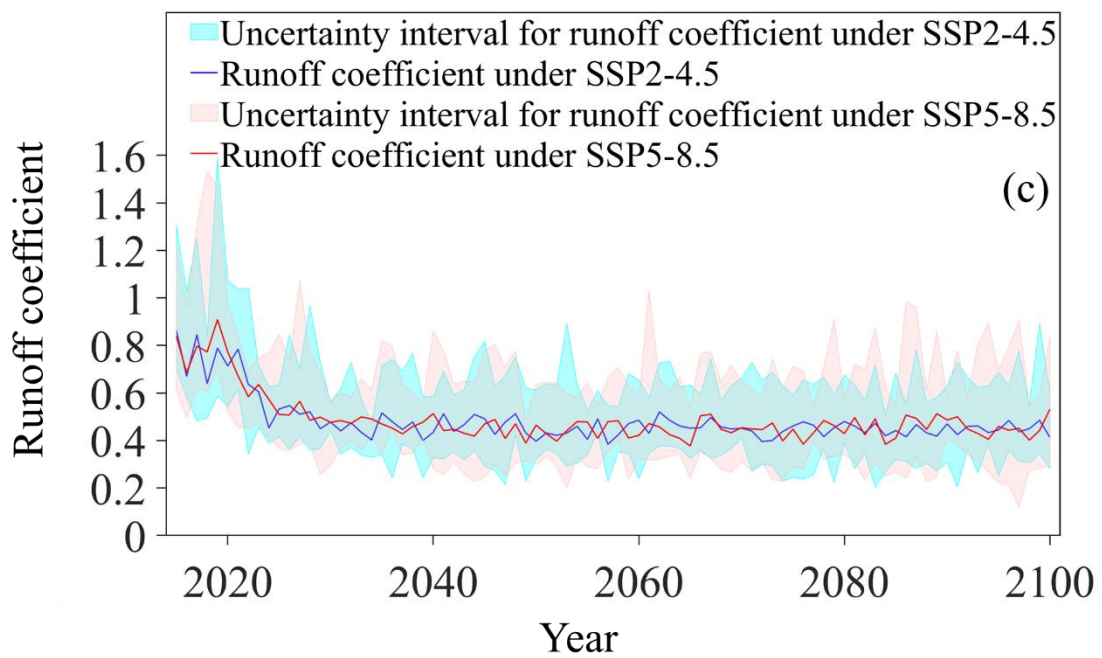
645 [in the non-glacier from 2015-2100](#)



646

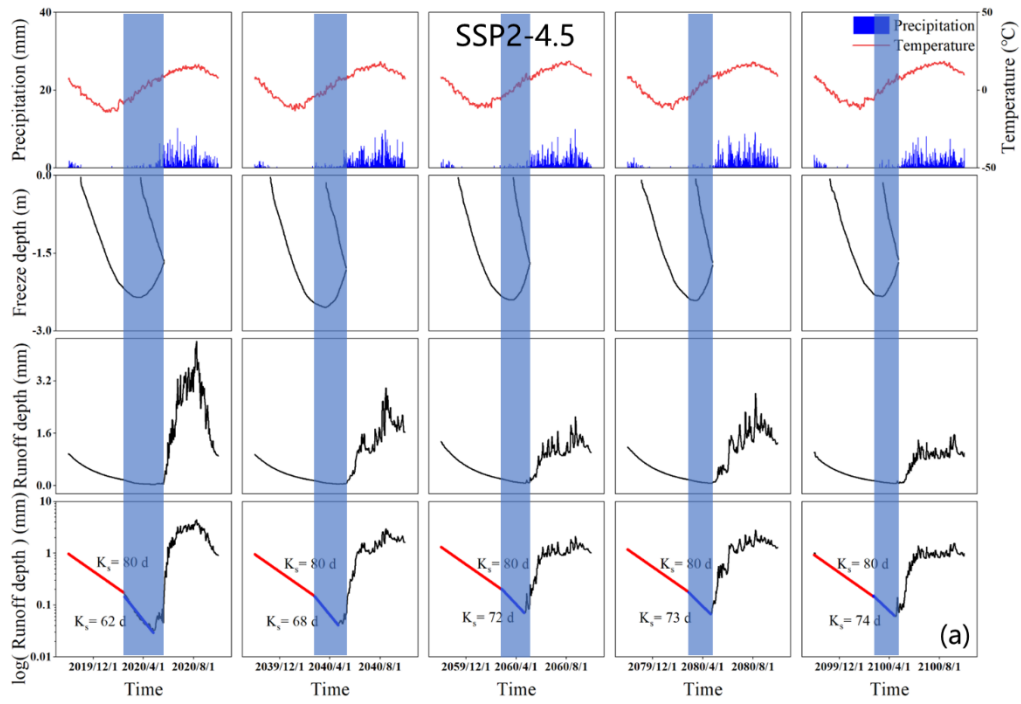


647

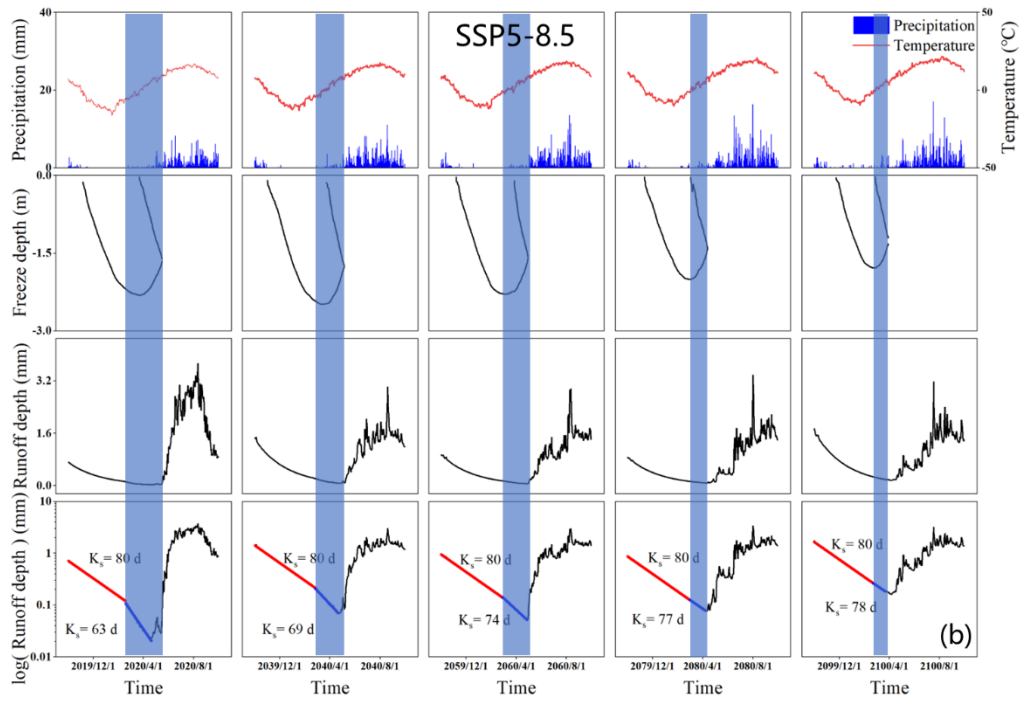


648

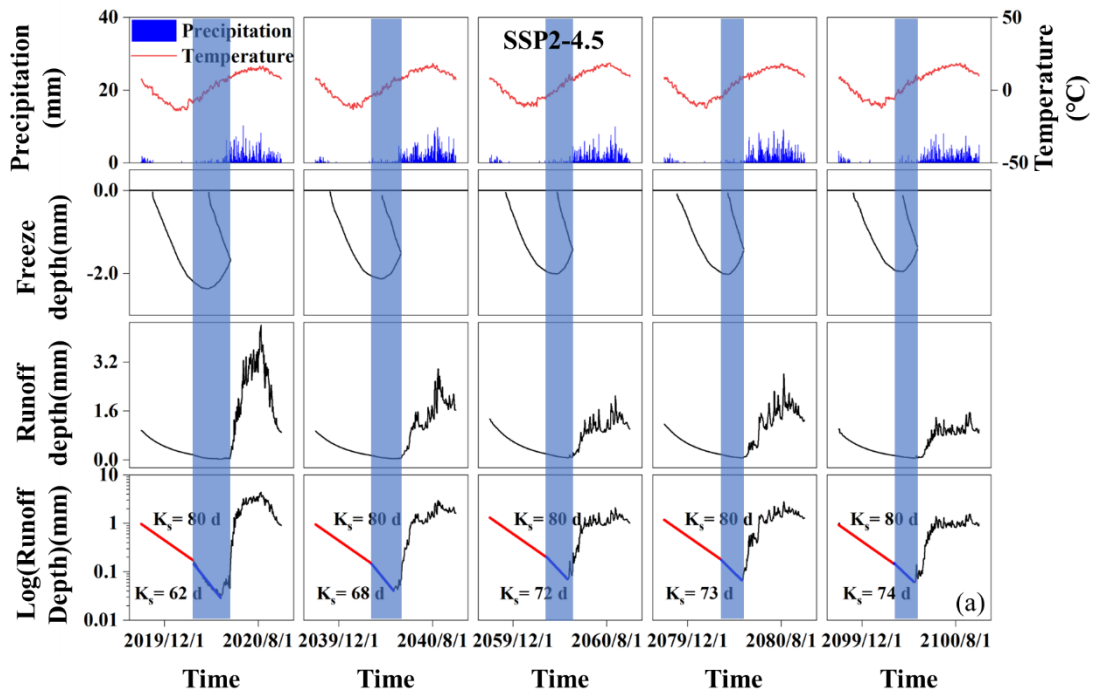
649 [Figure 11. \(a\) The predicted runoff depth of the total basin. \(b\) Runoff in the](#)
 650 [glacier and in the non-glacier from 2015-2100. \(c\) Project runoff coefficient under](#)
 651 [SSP2-4.5 and SSP5-8.5 scenarios.](#) ~~Figure 10. Project runoff coefficient under SSP2-~~
 652 ~~4.5 and SSP5-8.5 scenarios.~~



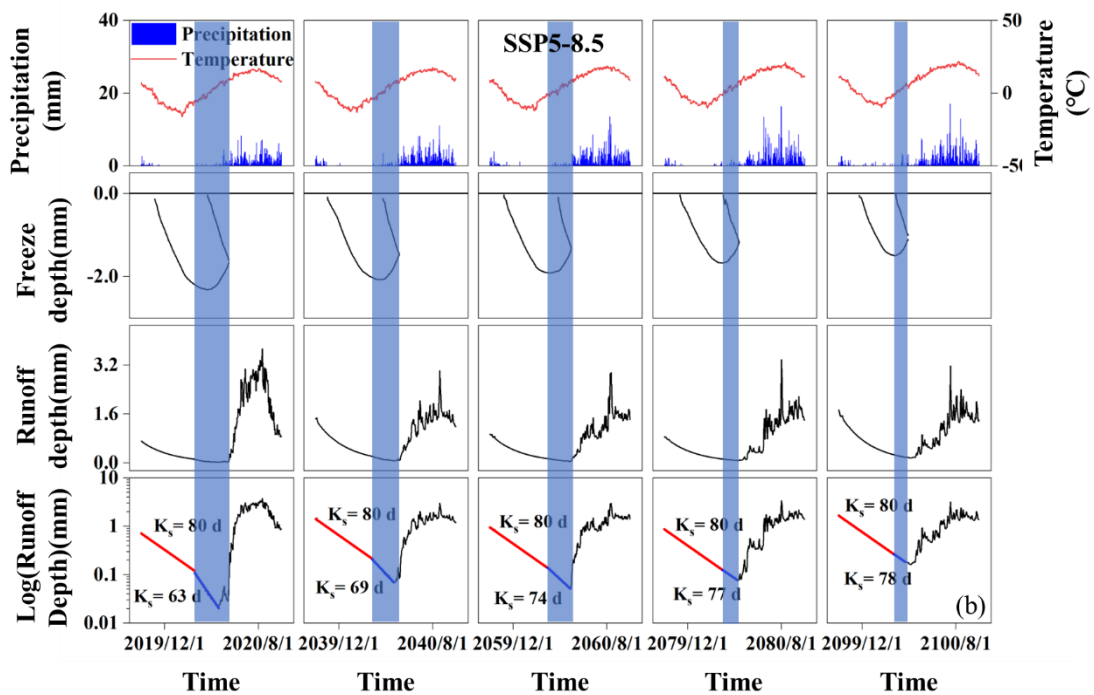
653



654



655



656

657 Figure 4.12. Temperature, precipitation, runoff depth and freeze-thaw cycle in
 658 2020, 2040, 2060, 2080 and 2100 under SSP2-4.5 (a, top) and SSP5-8.5 scenarios (b,
 659 bottom).

660 **5. Discussion**

5.1 Changes of the mountain cryosphere in future 5.1

The cryosphere, which encompasses glaciers, snow, frozen soil, and permafrost, plays a vital role in storing approximately 75% of the world's freshwater resources, while around 17% of the global population resides in cryosphere regions (Qin et al., 2021). Understanding the changes occurring in the cryosphere is crucial for assessing the long-term sustainability of water resources (Whitfield et al., 2021). The Hulu catchment, located in the northeast Tibet Plateau, exhibits a diverse distribution of cryosphere elements, making it an ideal area for studying these changes (Gao et al., 2019; Xu et al., 2019). However, there is a lack of research on the degradation of multiple cryosphere elements within the Hulu catchment and its implications for future hydrology, despite the Heihe River Basin being recognized as a typical region for studying hydrological and water resource changes in cold regions (Ning et al., 2008). In this study, we projected a future warming trend of 0.3°C per decade and 0.6°C per decade, accompanied by an increase in precipitation of 7.9 mm per decade and 12.0 mm per decade under the SSP2-4.5 and SSP5-8.5 scenarios, respectively (Figure 4). These projections align with the findings of Chen et al. (2022), who observed similar warming trends of 0.3–0.4 °C per decade and 0.7–0.8°C per decade, as well as precipitation increases ranging from 1.6–14.8 mm per decade and 6.0–20.6 mm per decade under similar scenarios. This consistency between our projections and previous research supports the reliability of the forcing data used in the FLEX-Cryo model.

Furthermore, Wang et al. (2018) predicted an increase in the annual maximum freeze depth in the Heihe River Basin from 2011 to 2066 at a rate of 5.4 cm per decade, which closely aligns with the predicted change of 5.2 cm per decade in our

685 study (Figure 6). While there have been limited studies investigating future changes in
686 glaciers and other cryosphere elements within the Hulu catchment, including the Shiyi
687 Glacier, conducting a comparative analysis with projections from other regions can
688 enhance our understanding of mountain cryosphere retreat. Although the comparative
689 analysis approach may have some limitations in terms of rigor, it provides valuable
690 insights (Han et al., 2023).

691 **5.2 The effect of the mountain cryosphere degradation on runoff**

692 Glaciers and snow are sensitive to climate change and cover play a crucial role in
693 water retention, with meltwater contributing significantly to downstream water
694 resources and the ecological environment (Stecher et al., 2023; Nan and Tian, 2024).
695 The turning point of glacier runoff represents a critical tipping point that signifies not
696 only the rapid thinning of glaciers but also the irreversible stage of water resources in
697 the basin (Brovkin et al., 2021). After the turning point the glacier thickness and glacier
698 volume rapidly decrease (Fig. 7). But the glacier thickness showed in this paper is the
699 change at the highest elevation band, which means the turning point would lag in this
700 band for change of glacier thickness. In the Hulu catchment, the proportion of glacier
701 runoff reached 51% to 55% between 2019 and 2021, indicating that it is in the turning
702 point period (~~Figure 9~~Fig. 11). Subsequently, the contribution of glacier runoff
703 gradually decreases until complete melting occurs. Temperature is the primary factor
704 influencing glacier runoff, while precipitation and temperature together determine the
705 proportion of glacier runoff in relation to total runoff. Although the highest contribution
706 of glacier runoff and the tipping point of glacier runoff may not align precisely, after
707 the tipping point, the capacity of glacier runoff to contribute to overall runoff
708 continuously diminishes. From 2015 to 2021, there has been a decreasing trend in

709 precipitation, leading to a corresponding decline in non-glacier runoff ([Figure 4](#)[Fig. 6](#)
710 and [9](#)[Fig. 11](#)). Thus, while glacier runoff has increased, the total runoff has decreased.
711 However, between 2032 and 2038, even though rainfall continues to decline, the
712 contribution of glacier runoff to overall runoff becomes negligible due to the limited
713 volume of ice remaining (glacier volume $< 1 \times 10^6 \text{ m}^3$), resulting in minimal glacier
714 melting runoff ([Figure 5](#)[Fig. 7](#) and [Figure 9](#)[Fig. 11](#)). On the other hand, once the glaciers
715 have completely melted, the total runoff in the Hulu catchment is reduced by 16% to
716 18%, and the runoff coefficient is halved ([Figure 9](#) and [Figure 10](#)). This
717 highlights the critical role of glaciers as solid freshwater reservoirs in regulating water
718 sources and mitigating droughts (McCarthy et al., 2022).

719 The freeze-thaw cycle has a significant impact on runoff yield and hydrological
720 response routines in the Hulu catchment (Sun et al., 2022; Wang et al., 2020).
721 Precipitation in the Hulu catchment is primarily concentrated in the summer when soil
722 moisture is high and even close to saturation, making saturation excess flow the main
723 mechanism for runoff generation (Li et al., 2016). During the freeze-thaw cycle, the
724 weak permeability of frozen soil affects both surface runoff and infiltration. Soil runoff
725 primarily occurs through underground in hillslope and surface water flow in riparian
726 area, resulting in a faster response to rainfall and snowmelt and contributing to a higher
727 runoff coefficient (Hu et al., 2022; Jones et al., 2023). However, it is important to note
728 that shallow frozen soil does not completely block the interaction between deeper soil
729 layers and the surface. Frost heave in the soil creates large pores, allowing snowmelt
730 water and precipitation to bypass the matrix layer and reach the deeper soils (Jiang et
731 al., 2021; Zhang et al., 2023). This phenomenon is considered one of the significant
732 reasons for low runoff in the early thawing season (Mohammed et al., 2021). Low

733 runoff is observed between the frozen season and complete thawing season ([Figure](#)
734 [+Fig. 12](#)). The duration of freeze-thaw cycles in [seasonal frozen soil](#)[seasonally frozen](#)
735 [soils](#) is shortening, and freeze onset is being delayed due to the warming climate,
736 resulting in a decreasing duration of low runoff. However, the temperature during the
737 freezing season remains lower than the initial frost heave temperature of the soil, and
738 there is still a deficit of soil water in the early thaw, indicating that the prevalence of
739 low runoff will persist in the future (Teng et al., 2022; Wen et al., 2024).

740 The freezing state has a significant impact on the recession process of baseflow,
741 and permafrost plays a crucial role in discontinuous baseflow (Cooper et al., 2023; J.
742 Wang et al., 2022). During the freezing season, baseflow follows a linear recession
743 process ($K_s = 80$ days), with contributions from both permafrost and [seasonal frozen](#)
744 [soil](#)[seasonally frozen soil](#) regions ([Figure](#) [+Fig. 12](#)). In the frozen season, the
745 groundwater under the supra-permafrost layer becomes inactive, and baseflow is solely
746 derived from the [seasonal frozen soil](#)[seasonally frozen soil](#) regions, causing a
747 discontinuous recession. With climate warming, the lower limit of permafrost gradually
748 moves upward along the elevation, resulting in the shrinking of the permafrost region.
749 This suggests that in the future, an increased proportion of baseflow will originate from
750 the expanding area of [seasonal frozen soil](#)[seasonally frozen soil](#), leading to a gradual
751 decrease in the influence of permafrost on baseflow. Consequently, the discontinuous
752 recession of baseflow will gradually transition into a linear recession. Furthermore, an
753 increase in the thickness of the active layer enhances the soil water storage capacity,
754 contributing to a gradual rise in baseflow (Yao et al., 2021).

755 [5.2 Comparison with other studies](#)

756 [The cryosphere, which encompasses](#)[including glaciers \(ice sheets\), seasonal snow](#)

757 cover, frozen soil, and permafrost, plays a vital role in storing approximately 75% of
758 the world's freshwater resources, while around 17% of the global population resides in
759 cryosphere regions (Qin et al., 2021). Although there are some differences in the the
760 driving data and models, the trends of the cryospheric elements and runoff changes are
761 still comparable and consistent. In this study, the small glaciers are projected to will
762 completely melt in the Mid-21st century, which is also reported this discovery in the
763 other area (Mukhopadhyay and Khan, 2015; Baraer et al., 2012; Schwank et al., 2014).
764 The projected maximum freeze depth of seasonally frozen soil calculated in this
765 research is 5.2 cm per decade, similar to is similar with the 5.4 cm per decade predicted
766 by Wang et al. (2018). Ni et al. (-2021) showed that Qinghai-Tibet Plateau permafrost
767 is at suffering from the risk of disappearance based on statistical and machine learning
768 (ML) modeling approaches. This shift in regions with permafrost impacts hydrological
769 connectivity, fostering improved hydrothermal conditions that enhance vegetation
770 growth (Han and Menzel, 2022; Jin et al., 2022). There are fFew studies have focused
771 on the change of-in the snow cover days and snow water equivalent in on the hHeihe
772 river basin in the future, but many researches have indicated that the snow-free period
773 increases and the snow water equivalent decreases due to caused by climatic warming
774 in Tibet Plateau (Zhang and Ma, 2018). The reduction of the snow cover period may
775 result in an earlier peak in spring snowmelt floods, thereby increasing the risk of
776 flooding (Chai et al., 2022). Simultaneously, the decrease in snow water equivalent may
777 impact plant water supply, placing pressure on ecosystems (Guan et al., 2022).
778 Although cryospheric elements have a trend of degradation in different regions, the
779 impact on runoff may be differentdiffer. However, But-on a longer time scale, the
780 degradation of the cryosphere will lead to a decrease in runoff decrease (Xu et al., 2024).

~~This study confirmed that;~~ runoff from cryospheric melting is one of the main factors controlling runoff, and degradation of the cryosphere may exacerbate the risk of future droughts.

5.3 Uncertainty and limitations

~~The uncertainty in this study arises from the forcing data of the General Circulation Models (GCMs), the bias correction methods, and the parameters selected in the FLEX-Cryo model (Wilby and Harris, 2006). The coarse spatial resolution of the GCMs prevents a comprehensive description of the climate at the basin scale, particularly in plateau and mountainous regions heavily influenced by altitude. The selection of parameters for the FLEX-Cryo model is also a significant source of uncertainties. Due to the complex topography in the mountain cryosphere, degree day factor, altitude effect on climate and soil water storage capacity cannot be fully reflected at the catchment scale. To mitigate some of the uncertainties associated with the GCM outputs, a multi-model and multi-method approach is employed in this study. The equal weighted average method is used to combine the values from different models and methods, aiming to reduce uncertainties and provide a more robust assessment of the results. It is important to note that the optimal parameter group selected for the FLEX-Cryo model in this study has been chosen based on previous research.~~
The sources of uncertainty in this study comes from the GCMs, the downscaling and bias correction methods, and the structure and parameters of the FLEX-Cryo model. The temperature and precipitation projections are uncertainty from different GCMs at the basin scale introduce uncertainty. Moreover, four bias correction methods were used to correct conduct a correction of the GCMs based on the observation, which may ensure consistent relative trends but not improve the accuracy of precipitation and temperature

805 frequency distribution and seasonal variations. This may cause some uncertainty in
806 the simulation results (Jia et al., 2023).

807 In this research, the time-variant albedo information and the aspect are worthwhile
808 to be taken into account for ~~to~~ improving glacier melting simulations, which need
809 require further observation and quantitative studies (Arnold et al., 2006; Feng et al.,
810 2024). The change of ~~in~~ elements in the cryosphere is sensitive to energy. The snow
811 cover and the effect of topographic shading may also have an effect on the degradation
812 and thus hydrologic response, which is worth ~~towards~~ further investigation (Zhang,
813 2005). On a long time scale, the degradation of frozen soil and glacier may result in ~~the~~
814 thaw lake generation and ~~the~~ other landscapes changes, which may effect on the runoff
815 yield and baseflow recession (Serban et al., 2021).

816 ~~(Gao et al., 2022). While this helps to establish a more reliable parameterization,~~
817 ~~there may still be inherent limitations in the chosen parameter values. Overall, the~~
818 ~~uncertainties and limitations associated with the forcing data, bias correction methods,~~
819 ~~and parameter selection in the FLEX-Cryo model need to be considered when~~
820 ~~interpreting the results of this study. Further research and improvements in these areas~~
821 ~~can enhance the accuracy and reliability of future assessments of the effects of~~
822 ~~mountain cryosphere degradation on runoff.~~

823 **6. Conclusions**

824 ~~The mountain cryosphere, encompassing glaciers, snow, and frozen soil, plays a~~
825 ~~critical role in downstream water resources and the ecological environment.~~
826 ~~Understanding its response to climate change is crucial for effective water resource~~
827 ~~management and flood prevention.~~ In this study, we employed the FLEX-Cryo model
828 and data from eight Global Climate Models (GCMs) under the SSP2-4.5 and SSP5-8.5

829 scenarios to ~~predict~~ the potential impacts of climate change on the mountain
830 cryosphere and hydrology. ~~Based on our simulation results, the following conclusions~~
831 ~~can be drawn:~~ Results from the projected change of mountain cryosphere elements,
832 glacier, snow and frozen soil are expected to undergo degradation. The glacier will
833 completely melt by the middle of the 21st century. Snow cover day will decrease by 45
834 and 76 days, and snow water equivalent will decrease by 0.24mm/yr and 0.35mm/yr.
835 The thaw onset is expected to advance 19 days and 32 days. The active layer thickness
836 will increase by 8.24cm/10yr.

837 (1) ~~The air temperature is projected to increase by 2.1 °C and 5 °C by 2100,~~
838 ~~while precipitation is expected to increase by 8 mm/10 years and 12 mm/10 years.~~
839 ~~These changes in temperature and precipitation patterns indicate a significant shift in~~
840 ~~the climatic conditions of the study area.~~

841 (2) ~~Glacier and snow cover are anticipated to experience retreat and shrinkage in the~~
842 ~~future. Under the SSP5-8.5 and SSP2-4.5 scenarios, glaciers are projected to~~
843 ~~completely melt by 2045 and 2051, respectively. Additionally, the duration of snow~~
844 ~~cover will be shortened by 45 days and 76 days, while the snow water equivalent will~~
845 ~~decrease by 0.24 mm/yr and 0.35 mm/yr.~~

846 (3) ~~The frozen soil is expected to undergo degradation. By 2100, the freeze onset of~~
847 ~~seasonal frozen soil is projected to delay by 10 days and 22 days, and the thaw onset~~
848 ~~of permafrost is expected to advance by 19 days and 32 days. The lower limit of~~
849 ~~permafrost is estimated to reach altitudes of 4015 m and 4355 m along the altitudinal~~
850 ~~gradient. Moreover, the maximum freeze depth will decrease by approximately 5.17~~
851 ~~cm/10 years and 10.93 cm/10 years, while the active layer thickness will increase by~~
852 ~~8.24 cm/10 years and 15.47 cm/10 years.~~

853 ~~(4) The degradation of the of the~~ mountain cryosphere has significant implications
854 for water ~~resources in the catchment area, particularly in terms of runoff yield.~~ resources.
855 The tipping point ~~for of~~ glacier runoff is projected to ~~occurred between 2019 and~~
856 2021. ~~occur in the 2020s.~~ Once the glaciers have completely melted, the ~~depth of~~ runoff
857 is projected to decrease by approximately 16% and 18% under the SSP2-4.5 and SSP5-
858 8.5 scenarios, respectively. ~~However, in non-glacier areas, the depth of runoff is~~
859 ~~expected to increase by 0.22 mm/yr and 1.07 mm/yr from 2015 to 2100. By the end of~~
860 ~~the 21st century, the runoff coefficient in the catchment is projected to reach~~
861 ~~approximately 0.42.~~ Importantly, the duration of low runoff ~~during the early thawing~~
862 ~~season will be shorter. The discontinuous~~ will shorten, baseflow will increase and the
863 discontinue recession of baseflow will is ~~gradually transitioning towards a~~ transform to
864 a more linear pattern ~~pattern, resulting in increased baseflow. The second recession~~
865 ~~coefficients are estimated to be around 74 days and 78 days, respectively, by the year~~
866 2100.

867 ~~In conclusion, this~~ This study provides insights into the potential impacts of
868 climate change on the mountain cryosphere and hydrology. The projected changes in
869 ~~temperature, precipitation,~~ glacier retreat, snow cover, and frozen soil dynamics
870 highlight the urgent need for proactive water resource management strategies in the
871 face of a changing climate. Further modelling research and monitoring efforts are
872 necessary to refine these projections and guide effective adaptation measures to
873 sustainably manage water resources in mountainous regions.

874

875 **Competing interests**

876 At least one of the (co-)authors is a member of the editorial board of Hydrology and

877 Earth System Sciences.

878

879 **Acknowledgements**

880 This research has been supported by the National Natural Science Foundation of China
881 (grant no. 42071081 and 42122002). Zheng Duan acknowledges the support from the
882 Crafoord Foundation (No. 20210552).

883

884 **References**

885 Abdelhamed, M. S., Elshamy, M. E., Wheeler, H. S., and Razavi, S.: Hydrologic-
886 land surface modelling of the Canadian sporadic-discontinuous permafrost:
887 Initialization and uncertainty propagation, *Hydrol. Process.*, 36,
888 <https://doi.org/10.1002/hyp.14509>, 2022.

889 Adler, C., Huggel, C., Orlove, B., and Nolin, A.: Climate change in the mountain
890 cryosphere: impacts and responses, *Reg Environ Change*, 19, 1225–1228,
891 <https://doi.org/10.1007/s10113-019-01507-6>, 2019.

892 Andrianaki, M., Shrestha, J., Kobierska, F., Nikolaidis, N. P., and Bernasconi, S.
893 M.: Assessment of SWAT spatial and temporal transferability for a high-altitude
894 glacierized catchment, *Hydrol. Earth Syst. Sci.*, 23, 3219–3232,
895 <https://doi.org/10.5194/hess-23-3219-2019>, 2019.

896 Arendt, A., Krakauer, N., Kumar, S. V., Rounce, D. R., and Rupper, S.: Editorial:
897 Collaborative Research to Address Changes in the Climate, Hydrology and Cryosphere
898 of High Mountain Asia, *Front. Earth Sci.*, 8, 605336,
899 <https://doi.org/10.3389/feart.2020.605336>, 2020.

900 [Arnold, N. S., Rees, W. G., Hodson, A. J., and Kohler, J.: Topographic controls on](#)

901 [the surface energy balance of a high Arctic valley glacier, J. Geophys. Res., 111,](#)
902 [2005JF000426, https://doi.org/10.1029/2005JF000426, 2006.](#)

903 [Aubry-Wake, C. and Pomeroy, J. W.: Predicting Hydrological Change in an Alpine](#)
904 [Glacierized Basin and Its Sensitivity to Landscape Evolution and Meteorological](#)
905 [Forcings, Water Resour. Res., 59, https://doi.org/10.1029/2022WR033363, 2023.](#)

906 [Baraer, M., Mark, B. G., McKenzie, J. M., Condom, T., Bury, J., Huh, K.-I.,](#)
907 [Portocarrero, C., Gómez, J., and Rathay, S.: Glacier recession and water resources in](#)
908 [Peru's Cordillera Blanca, J. Glaciol., 58, 134–150,](#)
909 [https://doi.org/10.3189/2012JoG11J186, 2012.](#)

910 Blöschl, G., Bierkens, M. F. P., Chambel, A., Cudennec, C., Destouni, G., Fiori,
911 A., Kirchner, J. W., McDonnell, J. J., Savenije, H. H. G., Sivapalan, M., Stump, C.,
912 Toth, E., Volpi, E., Carr, G., Lupton, C., Salinas, J., Széles, B., Viglione, A., Aksoy, H.,
913 Allen, S. T., Amin, A., Andréassian, V., Arheimer, B., Aryal, S. K., Baker, V., Bardsley,
914 E., Barendrecht, M. H., Bartosova, A., Batelaan, O., Berghuijs, W. R., Beven, K., Blume,
915 T., Bogaard, T., Borges De Amorim, P., Böttcher, M. E., Boulet, G., Breinl, K., Brilly,
916 M., Brocca, L., Buytaert, W., Castellarin, A., Castelletti, A., Chen, X., Chen, Y., Chen,
917 Y., Chiffard, P., Claps, P., Clark, M. P., Collins, A. L., Croke, B., Dathe, A., David, P.
918 C., De Barros, F. P. J., De Rooij, G., Di Baldassarre, G., Driscoll, J. M., Duethmann, D.,
919 Dwivedi, R., Eris, E., Farmer, W. H., Feiccabrino, J., Ferguson, G., Ferrari, E., Ferraris,
920 S., Fersch, B., Finger, D., Foglia, L., Fowler, K., Gartsman, B., Gascoin, S., Gaume, E.,
921 Gelfan, A., Geris, J., Gharari, S., Gleeson, T., Glendell, M., Gonzalez Bevacqua, A.,
922 González-Dugo, M. P., Grimaldi, S., Gupta, A. B., Guse, B., Han, D., Hannah, D.,
923 Harpold, A., Haun, S., Heal, K., Helfricht, K., Herrnegger, M., Hipsey, M., Hlaváčiková,
924 H., Hohmann, C., Holko, L., Hopkinson, C., Hrachowitz, M., Illangasekare, T. H., Inam,

925 A., Innocente, C., Istanbuluoglu, E., Jarihani, B., et al.: Twenty-three unsolved
926 problems in hydrology (UPH) – a community perspective, *Hydrology. Sci. J.*, 64, 1141–
927 1158, <https://doi.org/10.1080/02626667.2019.1620507>, 2019.

928 Bolibar, J., Rabatel, A., Gouttevin, I., Zekollari, H., and Galiez, C.: Nonlinear
929 sensitivity of glacier mass balance to future climate change unveiled by deep learning,
930 *Nat. Commun.*, 13, 409, <https://doi.org/10.1038/s41467-022-28033-0>, 2022.

931 Brovkin, V., Brook, E., Williams, J. W., Bathiany, S., Lenton, T. M., Barton, M.,
932 DeConto, R. M., Donges, J. F., Ganopolski, A., McManus, J., Praetorius, S., De Vernal,
933 A., Abe-Ouchi, A., Cheng, H., Claussen, M., Crucifix, M., Gallopín, G., Iglesias, V.,
934 Kaufman, D. S., Kleinen, T., Lambert, F., Van Der Leeuw, S., Liddy, H., Loutre, M.-F.,
935 McGee, D., Rehfeld, K., Rhodes, R., Seddon, A. W. R., Trauth, M. H., Vanderveken,
936 L., and Yu, Z.: Past abrupt changes, tipping points and cascading impacts in the Earth
937 system, *Nat. Geosci.*, 14, 550–558, <https://doi.org/10.1038/s41561-021-00790-5>, 2021.

938 Chadburn, S. E., Burke, E. J., Cox, P. M., Friedlingstein, P., Hugelius, G., and
939 Westermann, S.: An observation-based constraint on permafrost loss as a function of
940 global warming, *Nature Clim. Change*, 7, 340–344,
941 <https://doi.org/10.1038/nclimate3262>, 2017.

942 [Chai, C., Wang, L., Chen, D., Zhou, J., Liu, H., Zhang, J., Wang, Y., Chen, T., and](#)
943 [Liu, R.: Future snow changes and their impact on the upstream runoff in Salween,](#)
944 [Hydrol. Earth Syst. Sci.](#), 26, 4657–4683, <https://doi.org/10.5194/hess-26-4657-2022>,
945 [2022.](#)

946 Chang, Z., Qi, P., Zhang, G., Sun, Y., Tang, X., Jiang, M., Sun, J., and Li, Z.:
947 Latitudinal characteristics of frozen soil degradation and their response to climate
948 change in a high-latitude water tower, *CATENA*, 214, 106272,

949 <https://doi.org/10.1016/j.catena.2022.106272>, 2022.

950 [Chen, R., Duan, K., Shang, W., Shi, P., Meng, Y., and Zhang, Z.: Increase in](#)
951 [seasonal precipitation over the Tibetan Plateau in the 21st century projected using](#)
952 [CMIP6 models, Atmospheric Research, 277, 106306,](#)
953 <https://doi.org/10.1016/j.atmosres.2022.106306>, 2022

954 ~~Chen, R. S., Lu, S.-H., Kang, E.~~~~Chen, R., S., Lu, S.-H., Kang, E.-S.,~~ Ji, X., Zhang,
955 Z., Yang, Y., and Qing, W.: A distributed water-heat coupled model for mountainous
956 watershed of an inland river basin of Northwest China (I) model structure and equations,
957 Environ. Geol., 53, 1299–1309, <https://doi.org/10.1007/s00254-007-0738-2>, 2008.

958 ~~Chen, Z., Zhu, R., Yin, Z., Feng, Q., Yang, L., Wang, L., Lu, R., and Fang, C.:~~
959 ~~Hydrological response to future climate change in a mountainous watershed in~~
960 ~~the Northeast of Tibetan Plateau, Journal of Hydrology: Regional Studies, 44,~~
961 ~~101256, https://doi.org/10.1016/j.ejrh.2022.101256, 2022.~~

962 Connon, R. F., Chasmer, L., Haughton, E., Helbig, M., Hopkinson, C., Sonnentag,
963 O., and Quinton, W. L.: The implications of permafrost thaw and land cover change on
964 snow water equivalent accumulation, melt and runoff in discontinuous permafrost
965 peatlands, Hydrol. Process., 35, e14363, <https://doi.org/10.1002/hyp.14363>, 2021.

966 Cooper, M. G., Zhou, T., Bennett, K. E., Bolton, W. R., Coon, E. T., Fleming, S.
967 W., Rowland, J. C., and Schwenk, J.: Detecting Permafrost Active Layer Thickness
968 Change From Nonlinear Baseflow Recession, Water Resour. Res, 59,
969 <https://doi.org/10.1029/2022WR033154>, 2023.

970 Cullen, N. J., Sirguey, P., Mölg, T., Kaser, G., Winkler, M., and Fitzsimons, S. J.:
971 A century of ice retreat on Kilimanjaro: the mapping reloaded, The Cryosphere, 7, 419–
972 431, <https://doi.org/10.5194/tc-7-419-2013>, 2013.

973 Ding, Y., Zhang, S., Zhao, L., Li, Z., and Kang, S.: Global warming weakening the

974 inherent stability of glaciers and permafrost, *Sci. Bull.*, 64, 245–253,
975 <https://doi.org/10.1016/j.scib.2018.12.028>, 2019.

976 Ding, Y., Zhang, S., and Chen, R.: Cryospheric Hydrology: Decode the Largest
977 Freshwater Reservoir on Earth, *Bulletin of the Chinese Academy of Sciences*, 35, 414–
978 424, 2020.

979 Elshamy, M. E., Princz, D., Sapriza-Azuri, G., Abdelhamed, M. S., Pietroniro, A.,
980 Wheeler, H. S., and Razavi, S.: On the configuration and initialization of a large-scale
981 hydrological land surface model to represent permafrost, *Hydrol. Earth Syst. Sci.*, 24,
982 349–379, <https://doi.org/10.5194/hess-24-349-2020>, 2020.

983 Farinotti, D., Huss, M., Fürst, J. J., Landmann, J., Machguth, H., Maussion, F., and
984 Pandit, A.: A consensus estimate for the ice thickness distribution of all glaciers on
985 Earth, *Nat. Geosci.*, 12, 168–173, <https://doi.org/10.1038/s41561-019-0300-3>, 2019.

986 [Feng, S., Cook, J. M., Naegeli, K., Anesio, A. M., Benning, L. G., and Tranter, M.:
987 The Impact of Bare Ice Duration and Geo - Topographical Factors on the Darkening of
988 the Greenland Ice Sheet, *Geophysical Research Letters*, 51, e2023GL104894,
989 <https://doi.org/10.1029/2023GL104894>, 2024.](https://doi.org/10.1029/2023GL104894)

990 Fenicia, F. and McDonnell, J. J.: Modeling streamflow variability at the regional
991 scale: (1) perceptual model development through signature analysis, *J. Hydrol.*, 605,
992 127287, <https://doi.org/10.1016/j.jhydrol.2021.127287>, 2022.

993 Gao, H., ~~Wang, J., Yang, Y., Pan, X., Ding, Y., and Duan, Z.: Permafrost Hydrology of
994 the Qinghai-Tibet Plateau: A Review of Processes and Modeling, *FRONT
995 EARTH SCI*, 8, <https://doi.org/10.3389/feart.2020.576838>, 2021.~~

996 ~~Gao, H.,~~ Han, C., Chen, R., Feng, Z., Wang, K., Fenicia, F., and Savenije, H.:
997 Frozen soil hydrological modeling for a mountainous catchment northeast of the
998 Qinghai-Tibet Plateau, *Hydrol. Earth Syst. Sci.*, 26, 4187–4208,

999 <https://doi.org/10.5194/hess-26-4187-2022>, 2022.

1000 [Gao, H., Feng, Z., Zhang, T., Wang, Y., He, X., Li, H., Pan, X., Ren, Z., Chen, X.,](#)
1001 [Zhang, W., and Duan, Z.: Assessing glacier retreat and its impact on water resources in](#)
1002 [a headwater of Yangtze River based on CMIP6 projections, Science of The Total](#)
1003 [Environment, 765, 142774, https://doi.org/10.1016/j.scitotenv.2020.142774, 2021.](#)

1004 [Gao, T., Kang, S., Chen, R., Zhang, T., Zhang, T., Han, C., Tripathee, L., Sillanpää,](#)
1005 [M., and Zhang, Y.: Riverine dissolved organic carbon and its optical properties in a](#)
1006 [permafrost region of the Upper Heihe River basin in the Northern Tibetan Plateau, Sci.](#)
1007 [Total Environ., 686, 370–381, https://doi.org/10.1016/j.scitotenv.2019.05.478, 2019.](#)

1008 [Gilg, O., Kovacs, K. M., Aars, J., Fort, J., Gauthier, G., Grémillet, D., Ims, R. A.,](#)
1009 [Meltofte, H., Moreau, J., Post, E., Schmidt, N. M., Yannic, G., and Bollache, L.: Climate](#)
1010 [change and the ecology and evolution of Arctic vertebrates, Ann. Ny. Acad. Sci., 1249,](#)
1011 [166–190, https://doi.org/10.1111/j.1749-6632.2011.06412.x, 2012.](#)

1012 [Giovando, J. and Niemann, J. D.: Wildfire Impacts on Snowpack Phenology in a](#)
1013 [Changing Climate Within the Western U.S., Water Resour. Res., 58, e2021WR031569,](#)
1014 [https://doi.org/10.1029/2021WR031569, 2022.](#)

1015 [Gisnås, K., Westermann, S., Schuler, T. V., Melvold, K., and Etzelmüller, B.:](#)
1016 [Small-scale variation of snow in a regional permafrost model, The Cryosphere, 10,](#)
1017 [1201–1215, https://doi.org/10.5194/tc-10-1201-2016, 2016.](#)

1018 [Guan, X., Guo, S., Huang, J., Shen, X., Fu, L., and Zhang, G.: Effect of seasonal](#)
1019 [snow on the start of growing season of typical vegetation in Northern Hemisphere,](#)
1020 [Geography and Sustainability, 3, 268–276,](#)
1021 [https://doi.org/10.1016/j.geosus.2022.09.001, 2022.](#)

1022 [Hamon, W.R.: Estimating potential evapotranspiration. J. Hydraul. Div.-ASCE 87,](#)

1023 [107–120, 1961.](#)

1024 Han, L. and Menzel, L.: Hydrological variability in southern Siberia and the role
1025 of permafrost degradation, *J. Hydrol.*, 604, 127203,
1026 <https://doi.org/10.1016/j.jhydrol.2021.127203>, 2022.

1027 ~~Han, P., Long, D., Zhao, F., and Slater, L. J.: Response of Two Glaciers in Different
1028 Climate Settings of the Tibetan Plateau to Climate Change Through Year 2100
1029 Using a Hybrid Modeling Approach, *Water Resour. Res.*, 59,
1030 <https://doi.org/10.1029/2022WR033618>, 2023.~~

1031 He, Q., Kuang, X., Chen, J., Hao, Y., Feng, Y., Wu, P., and Zheng, C.: Glacier
1032 retreat and its impact on groundwater system evolution in the Yarlung Zangbo source
1033 region, Tibetan Plateau, *J. Hydrol.: Regional Studies*, 47, 101368,
1034 <https://doi.org/10.1016/j.ejrh.2023.101368>, 2023.

1035 He, Z., Duethmann, D., and Tian, F.: A meta-analysis based review of quantifying
1036 the contributions of runoff components to streamflow in glacierized basins. *J. Hydrol.*,
1037 603, 126890, <https://doi.org/10.1016/j.jhydrol.2021.126890>, 2021.

1038 Hu, G., Li, X., Yang, X., Shi, F., Sun, H., and Cui, B.: Identifying Spatiotemporal
1039 Patterns of Hillslope Subsurface Flow in an Alpine Critical Zone on the Qinghai -
1040 Tibetan Plateau Based on Three - Year, High - Resolution Field Observations, *Water
1041 Resour. Res.*, 58, e2022WR032098, <https://doi.org/10.1029/2022WR032098>, 2022.

1042 Huss, M. and Fischer, M.: Sensitivity of Very Small Glaciers in the Swiss Alps to
1043 Future Climate Change, *Front. Earth Sci.*, 4, <https://doi.org/10.3389/feart.2016.00034>,
1044 2016.

1045 Huss, M. and Hock, R.: Global-scale hydrological response to future glacier mass
1046 loss, *Nature Clim Change*, 8, 135–140, <https://doi.org/10.1038/s41558-017-0049-x>,
1047 2018.

1048 Huss, M., Jouvét, G., Farinotti, D., and Bauder, A.: Future high-mountain
1049 hydrology: a new parameterization of glacier retreat, *Hydrol. Earth Syst. Sci.*, 14, 815–
1050 829, <https://doi.org/10.5194/hess-14-815-2010>, 2010.

1051 Intergovernmental Panel On Climate Change (Ipcc): The Ocean and Cryosphere
1052 in a Changing Climate: Special Report of the Intergovernmental Panel on Climate
1053 Change, 1st ed., Cambridge University Press, <https://doi.org/10.1017/9781009157964>,
1054 2022.

1055 [Jia, Q., Jia, H., Li, Y., and Yin, D.: Applicability of CMIP5 and CMIP6 Models in](#)
1056 [China: Reproducibility of Historical Simulation and Uncertainty of Future Projection,](#)
1057 [Journal of Climate, 36, 5809–5824, https://doi.org/10.1175/JCLI-D-22-0375.1, 2023.](#)

1058 Jiang, R., Li, T., Liu, D., Fu, Q., Hou, R., Li, Q., Cui, S., and Li, M.: Soil infiltration
1059 characteristics and pore distribution under freezing–thawing conditions, *The*
1060 *Cryosphere*, 15, 2133–2146, <https://doi.org/10.5194/tc-15-2133-2021>, 2021.

1061 [Jin, X., Jin, H., Luo, D., Sheng, Y., Wu, Q., Wu, J., Wang, W., Huang, S., Li, X.,](#)
1062 [Liang, S., Wang, Q., He, R., Serban, R. D., Ma, Q., Gao, S., and Li, Y.: Impacts of](#)
1063 [Permafrost Degradation on Hydrology and Vegetation in the Source Area of the Yellow](#)
1064 [River on Northeastern Qinghai-Tibet Plateau, Southwest China, Front. Earth Sci., 10,](#)
1065 [845824, https://doi.org/10.3389/feart.2022.845824, 2022.](#)

1066 Jones, M. W., Sebestyen, S. D., Dymond, S. F., Ng, G. H. C., and Feng, X.: Soil
1067 frost controls streamflow generation processes in headwater catchments, *J. Hydrol.*, 617,
1068 <https://doi.org/10.1016/j.jhydrol.2022.128801>, 2023.

1069 Kaplan Pastíriková, L., Hrbáček, F., Uxa, T., and Láska, K.: Permafrost table
1070 temperature and active layer thickness variability on James Ross Island, Antarctic
1071 Peninsula, in 2004–2021, *Sci. Total Environ.*, 869, 161690,

1072 <https://doi.org/10.1016/j.scitotenv.2023.161690>, 2023.

1073 Li, L., Xu, Z., Zuo, D., and Zhao, J.: A grid-based integrated surface–groundwater
1074 model (GISMOD), *J. Water Clim. Change*, 7, 296–320,
1075 <https://doi.org/10.2166/wcc.2015.006>, 2016.

1076 Li, X., Jin, H., Sun, L., Wang, H., Huang, Y., He, R., Chang, X., Yu, S., and Zang,
1077 S.: TTOP - model - based maps of permafrost distribution in Northeast China for
1078 1961 - 2020, *Permafrost periglac*, 33, 425–435, <https://doi.org/10.1002/ppp.2157>,
1079 2022.

1080 [Li, Z., Feng, Q., Chen, W., Wang, T., Cheng, Yan, G., Xiaoyan, G., Yanhui, P.,](#)
1081 [Jianguo, L., Rui, G., and Bing, J.: Study on the contribution of cryosphere to runoff in](#)
1082 [the cold alpine basin: A case study of Hulugou River Basin in the Qilian Mountains,](#)
1083 [Global and Planetary Change](#), 122, 345–361,
1084 <https://doi.org/10.1016/j.gloplacha.2014.10.001>, 2014.

1085 [Liu, J. and Chen, R.: Discriminating types of precipitation in Qilian Mountains,](#)
1086 [Tibetan Plateau, Journal of Hydrology: Regional Studies](#), 5, 20–32,
1087 <https://doi.org/10.1016/j.ejrh.2015.11.013>, 2016.

1088 Liu, Z., Cuo, L., and Sun, N.: Tracking snowmelt during hydrological surface
1089 processes using a distributed hydrological model in a mesoscale basin on the Tibetan
1090 Plateau, *J. Hydrol.*, 616, <https://doi.org/10.1016/j.jhydrol.2022.128796>, 2023.

1091 [Ma, J., Li, R., Huang, Z., Wu, T., Wu, X., Zhao, L., Liu, H., Hu, G., Xiao, Y., Du,](#)
1092 [Y., Yang, S., Liu, W., Jiao, Y., and Wang, S.: Evaluation and spatio-temporal analysis](#)
1093 [of surface energy flux in permafrost regions over the Qinghai-Tibet Plateau and Arctic](#)
1094 [using CMIP6 models, International Journal of Digital Earth](#), 15, 1947–1965,
1095 <https://doi.org/10.1080/17538947.2022.2142307>, 2022.

1096 [Martin, L. C. P., Westermann, S., Magni, M., Brun, F., Fiddes, J., Lei, Y.,](#)
1097 [Kraaijenbrink, P., Mathys, T., Langer, M., Allen, S., and Immerzeel, W. W.: Recent](#)
1098 [ground thermo-hydrological changes in a southern Tibetan endorheic catchment and](#)
1099 [implications for lake level changes, Hydrol. Earth Syst. Sci., 27, 4409–4436,](#)
1100 <https://doi.org/10.5194/hess-27-4409-2023>, 2023

1101 McCarthy, M., Meier, F., Fatichi, S., Stocker, B. D., Shaw, T. E., Miles, E.,
1102 Dussailant, I., and Pellicciotti, F.: Glacier Contributions to River Discharge During the
1103 Current Chilean Megadrought, Earth's Future, 10, e2022EF002852,
1104 <https://doi.org/10.1029/2022EF002852>, 2022.

1105 Michel, A., Schaefli, B., Wever, N., Zekollari, H., Lehning, M., and Huwald, H.:
1106 Future water temperature of rivers in Switzerland under climate change investigated
1107 with physics-based models, Hydrol. Earth Syst. Sci., 26, 1063–1087,
1108 <https://doi.org/10.5194/hess-26-1063-2022>, 2022.

1109 Miner, K., Turetsky, M., Malina, E., Bartsch, A., Tamminen, J., McGuire, A., Fix,
1110 A., Sweeney, C., Elder, C., and Miller, C.: Permafrost carbon emissions in a changing
1111 Arctic, Nature Reviews Earth & Environmental, 3, 55–67,
1112 <https://doi.org/10.1038/s43017-021-00230-3>, 2022.

1113 Mohammed, A. A., Cey, E. E., Hayashi, M., and Callaghan, M., V.: Simulating
1114 preferential flow and snowmelt partitioning in seasonally frozen hillslopes, Hydrol.
1115 Process., 35, <https://doi.org/10.1002/hyp.14277>, 2021.

1116 Moreno, P. I., Fercovic, E. I., Soteres, R. L., Ugalde, P. I., Sagredo, E. A., and
1117 Villa-Martínez, R. P.: Glacier and terrestrial ecosystem evolution in the Chilotan
1118 archipelago sector of northwestern Patagonia since the Last Glacial Termination, Earth-
1119 Science Reviews, 235, 104240, <https://doi.org/10.1016/j.earscirev.2022.104240>, 2022.

1120 [Mukhopadhyay, B. and Khan, A.: A reevaluation of the snowmelt and glacial melt](#)
1121 [in river flows within Upper Indus Basin and its significance in a changing climate,](#)
1122 [Journal of Hydrology, 527, 119–132, <https://doi.org/10.1016/j.jhydrol.2015.04.045>,](#)
1123 [2015.](#)

1124 [Nan, Y. and Tian, F.: Glaciers determine the sensitivity of hydrological processes](#)
1125 [to perturbed climate in a large mountainous basin on the Tibetan Plateau, Hydrol. Earth](#)
1126 [Syst. Sci., 28, 669–689, <https://doi.org/10.5194/hess-28-669-2024>, 2024.](#)

1127 Negi, V. S., Tiwari, D. C., Singh, L., Thakur, S., and Bhatt, I. D.: Review and
1128 synthesis of climate change studies in the Himalayan region, Environ Dev Sustain, 24,
1129 10471–10502, <https://doi.org/10.1007/s10668-021-01880-5>, 2022.

1130 [Ni, J., Wu, T., Zhu, X., Hu, G., Zou, D., Wu, X., Li, R., Xie, C., Qiao, Y., Pang, Q.,](#)
1131 [Hao, J., and Yang, C.: Simulation of the Present and Future Projection of Permafrost on](#)
1132 [the Qinghai - Tibet Plateau with Statistical and Machine Learning Models, JGR](#)
1133 [Atmospheres, 126, e2020JD033402, <https://doi.org/10.1029/2020JD033402>, 2021.](#)

1134 Nury, A. H., Sharma, A., Mehrotra, R., Marshall, L., and Cordery, I.: Projected
1135 Changes in the Tibetan Plateau Snowpack Resulting From Rising Global Temperatures,
1136 J. Geophys. Res.-Atmos. , 127, <https://doi.org/10.1029/2021JD036201>, 2022.

1137 [Peng, Z., Tian, F., Wu, J., Huang, J., Hu, H., and Darnault, C. J. G.: A numerical](#)
1138 [model for water and heat transport in freezing soils with nonequilibrium ice - water](#)
1139 [interfaces, Water Resources Research, 52, 7366 – 7381,](#)
1140 [https://doi.org/10.1002/2016WR019116, 2016.](#)

1141 Pomeroy, J. W., Brown, T., Fang, X., Shook, K. R., Pradhananga, D., Armstrong,
1142 R., Harder, P., Marsh, C., Costa, D., Krogh, S. A., Aubry-Wake, C., Annand, H.,
1143 Lawford, P., He, Z., Kompanizare, M., and Lopez Moreno, J. I.: The cold regions

1144 hydrological modelling platform for hydrological diagnosis and prediction based on
1145 process understanding, *J. Hydrol.*, 615, 128711,
1146 <https://doi.org/10.1016/j.jhydrol.2022.128711>, 2022.

1147 Pothula, S. K. and Adams, B. J.: Community assembly in the wake of glacial
1148 retreat: A meta - analysis, *Glob. Chang Biol*, 28, 6973–6991,
1149 <https://doi.org/10.1111/gcb.16427>, 2022.

1150 Qin, D., Yao, T., Ding, Y., and Ren, J.: Classification and Geographical
1151 Distribution of Cryosphere, in: *Introduction to Cryospheric Science*. Springer
1152 Singapore, Singapore, 33–79, https://doi.org/10.1007/978-981-16-6425-0_2, 2021.

1153 Rabatel, A., Ceballos, J. L., Micheletti, N., Jordan, E., Braitmeier, M., González,
1154 J., Mölg, N., Ménégoz, M., Huggel, C., and Zemp, M.: Toward an imminent extinction
1155 of Colombian glaciers?, *Geografiska Annaler: Series A, Phys Geog*, 100, 75–95,
1156 <https://doi.org/10.1080/04353676.2017.1383015>, 2018.

1157 Ragettli, S., Immerzeel, W. W., and Pellicciotti, F.: Contrasting climate change
1158 impact on river flows from high-altitude catchments in the Himalayan and Andes
1159 Mountains, *Proc. Natl. Acad. Sci. U.S.A.*, 113, 9222–9227,
1160 <https://doi.org/10.1073/pnas.1606526113>, 2016.

1161 Rasul, G., Pasakhala, B., Mishra, A., and Pant, S.: Adaptation to mountain
1162 cryosphere change: issues and challenges, *Clim Dev*, 12, 297–309,
1163 <https://doi.org/10.1080/17565529.2019.1617099>, 2020.

1164 Rosier, S. H. R., Reese, R., Donges, J. F., De Rydt, J., Gudmundsson, G. H., and
1165 Winkelmann, R.: The tipping points and early warning indicators for Pine Island Glacier,
1166 West Antarctica, *The Cryosphere*, 15, 1501–1516, [https://doi.org/10.5194/tc-15-1501-](https://doi.org/10.5194/tc-15-1501-2021)
1167 2021, 2021.

1168 [Schwank, J., Escobar, R., Girón, G. H., and Morán-Tejeda, E.: Modeling of the](#)
1169 [Mendoza river watershed as a tool to study climate change impacts on water availability,](#)
1170 [Environmental Science & Policy, 43, 91–97,](#)
1171 <https://doi.org/10.1016/j.envsci.2014.01.002>, 2014.

1172 [Serban, R., Jin, H., Serban, M., and Luo, D.: Shrinking thermokarst lakes and](#)
1173 [ponds on the northeastern Qinghai-Tibet plateau over the past three decades,](#)
1174 [PERMAFROST AND PERIGLACIAL PROCESSES, 32, 601–617,](#)
1175 <https://doi.org/10.1002/ppp.2127>, 2021.

1176 Stecher, G., Hohensinner, S., and Herrnegger, M.: Changes in the water retention
1177 of mountainous landscapes since the 1820s in the Austrian Alps, *Front. Environ. Sci.*,
1178 11, 1219030, <https://doi.org/10.3389/fenvs.2023.1219030>, 2023.

1179 Sun, B., Liu, J., Ren, F., Li, H., Zhang, G., Ma, J., Ma, B., and Li, Z.: Effects of
1180 seasonal freeze–thaw and wind erosion on runoff and sediment yields of three loamy
1181 slopes of Loess Plateau, China, *CATENA*, 215, 106309,
1182 <https://doi.org/10.1016/j.catena.2022.106309>, 2022.

1183 Tang, G., Clark, M. P., Knoben, W. J. M., Liu, H., Gharari, S., Arnal, L., Beck, H.
1184 E., Wood, A. W., Newman, A. J., and Papalexiou, S. M.: The Impact of Meteorological
1185 Forcing Uncertainty on Hydrological Modeling: A Global Analysis of Cryosphere
1186 Basins, *Water Resour. Res*, 59, e2022WR033767,
1187 <https://doi.org/10.1029/2022WR033767>, 2023.

1188 Teng, J., Liu, J., Zhang, S., and Sheng, D.: Frost heave in coarse-grained soils:
1189 experimental evidence and numerical modelling, *GEOTECHNIQUE*, 73, 1100–1111,
1190 <https://doi.org/10.1680/jgeot.21.00182>, 2022.

1191 Teutschbein, C. and Seibert, J.: Bias correction of regional climate model

1192 simulations for hydrological climate-change impact studies: Review and evaluation of
1193 different methods, *J. Hydrol.*, 456–457, 12–29,
1194 <https://doi.org/10.1016/j.jhydrol.2012.05.052>, 2012.

1195 Van Der Geest, K. and Van Den Berg, R.: Slow-onset events: a review of the
1196 evidence from the IPCC Special Reports on Land, Oceans and Cryosphere, *CURR*
1197 *OPIN ENV SUST*, 50, 109–120, <https://doi.org/10.1016/j.cosust.2021.03.008>, 2021.

1198 Vincent, C. and Thibert, E.: Brief communication: Non-linear sensitivity of glacier
1199 mass balance to climate attested by temperature-index models, *The Cryosphere*, 17,
1200 1989–1995, <https://doi.org/10.5194/tc-17-1989-2023>, 2023.

1201 Wang, J., Chen, X., Gao, M., Hu, Q., and Liu, J.: Changes in nonlinearity and
1202 stability of streamflow recession characteristics under climate warming in a large
1203 glaciated basin of the Tibetan Plateau, *Hydrol. Earth Syst. Sci.*, 26, 3901–3920,
1204 <https://doi.org/10.5194/hess-26-3901-2022>, 2022a.

1205 Wang, K., Zhang, T., and Clow, G. D.: Permafrost Thermal Responses to
1206 Asymmetrical Climate Changes: An Integrated Perspective, *Geophys. Res. Lett.*, 50,
1207 e2022GL100327, <https://doi.org/10.1029/2022GL100327>, 2023.

1208 Wang, Q., Qi, J., Wu, H., Zeng, Y., Shui, W., Zeng, J., and Zhang, X.: Freeze-Thaw
1209 cycle representation alters response of watershed hydrology to future climate change,
1210 *CATENA*, 195, <https://doi.org/10.1016/j.catena.2020.104767>, 2020.

1211 Wang, S., Yang, Y., and Che, Y.: Global Snow- and Ice-Related Disaster Risk: A
1212 Review, *Nat. Hazards Rev.*, 23, 03122002, [https://doi.org/10.1061/\(ASCE\)NH.1527-6996.0000584](https://doi.org/10.1061/(ASCE)NH.1527-6996.0000584), 2022b.

1214 Wang, X., Chen, R., Liu, G., Yang, Y., Song, Y., Liu, J., Liu, Z., Han, C., Liu, X.,
1215 Guo, S., Wang, L., and Zheng, Q.: Spatial distributions and temporal variations of the

1216 near-surface soil freeze state across China under climate change, *Global Planetary*
1217 *Change*, 172, 150–158, <https://doi.org/10.1016/j.gloplacha.2018.09.016>, 2019.

1218 Wang, Y., Yang, H., Gao, B., Wang, T., Qin, Y., and Yang, D.: Frozen ground
1219 degradation may reduce future runoff in the headwaters of an inland river on the
1220 northeastern Tibetan Plateau, *J. Hydrol.*, 564, 1153–1164,
1221 <https://doi.org/10.1016/j.jhydrol.2018.07.078>, 2018.

1222 Wei, L., Zhao, W., Feng, X., Han, C., Li, T., Qi, J., and Li, Y.: Freeze-thaw
1223 desertification of alpine meadow in Qilian Mountains and the implications for alpine
1224 ecosystem management, *CATENA*, 232, 107471,
1225 <https://doi.org/10.1016/j.catena.2023.107471>, 2023.

1226 Wen, Y., Liu, B., Jiang, H., Li, T.-Y., Zhang, B., and Wu, W.: Initial soil moisture
1227 prewinter affects the freeze–thaw profile dynamics of a Mollisol in Northeast China,
1228 *CATENA*, 234, 107648, <https://doi.org/10.1016/j.catena.2023.107648>, 2024.

1229 ~~[Whitfield, P. H., Kraaijenbrink, P. D. A., Shook, K. R., and Pomeroy, J. W.: The](#)~~
1230 ~~[spatial extent of hydrological and landscape changes across the mountains and](#)~~
1231 ~~[prairies of Canada in the Mackenzie and Nelson River basins based on data from](#)~~
1232 ~~[a warm season time window, *Hydrol. Earth Syst. Sci.*, 25, 2513–2541,](#)~~
1233 ~~<https://doi.org/10.5194/hess-25-2513-2021>,~~

1234 Wiersma, P., Aerts, J., Zekollari, H., Hrachowitz, M., Drost, N., Huss, M.,
1235 Sutanudjaja, E. H., and Hut, R.: Coupling a global glacier model to a global
1236 hydrological model prevents underestimation of glacier runoff, *Hydrol. Earth Syst. Sci.*,
1237 26, 5971–5986, <https://doi.org/10.5194/hess-26-5971-2022>, 2022.

1238 ~~[Wilby, R. L. and Harris, I.: A framework for assessing uncertainties in climate](#)~~
1239 ~~[change impacts: Low – flow scenarios for the River Thames, UK, Xing, Z. P., Zhao, L.,](#)~~
1240 ~~[Fan, L., Hu, G. J., Zou, D. F., Wang, C., Liu, S. C., Du, E. J., Xiao, Y., Li, R., Liu, G.](#)~~

1241 [Y., Qiao, Y. P., and Shi, J. Z.: Changes in the ground surface temperature in permafrost](#)
1242 [regions along the Qinghai–Tibet engineering corridor from 1900 to 2014: A modified](#)
1243 [assessment of CMIP6, *Advances in Climate Change Research*, 14, 85–96,](#)
1244 <https://doi.org/10.1016/j.accre.2023.01.007>, 2023.

1245 [Xu, P., Yan, D., Weng, B., Bian, J., Wu, C., and Wang, H.: Evolution trends and](#)
1246 [driving factors of groundwater storage, recharge, and discharge in the Qinghai-Tibet](#)
1247 [Plateau: Study progress and challenges, *Journal of Hydrology*, 631, 130815,](#)
1248 <https://doi.org/10.1016/j.jhydrol.2024.130815>, 2024.

1249 ~~[Water Resour. Res](#), 42, 2005WR004065, <https://doi.org/10.1029/2005WR004065>,~~
1250 ~~2006.~~

1251 ~~[Xu, C., Li, Z., Wang, F., Ha, L., Yagoub, Y. E., and Jin, S.: Recent geodetic mass](#)~~
1252 ~~[balance and extent changes of very small glaciers in the Hulugou Basin, Central](#)~~
1253 ~~[Qilian Mountains, China, *J Earth Syst Sci*, 128, 47,](#)~~
1254 ~~<https://doi.org/10.1007/s12040-019-1067-z>, 2019.~~

1255 Yang, M., Li, Z., Anjum, M. N., Kayastha, R., Kayastha, R. B., Rai, M., Zhang,
1256 X., and Xu, C.: Projection of Streamflow Changes Under CMIP6 Scenarios in the
1257 Urumqi River Head Watershed, Tianshan Mountain, China, *Front. Earth Sci.*, 10,
1258 857854, <https://doi.org/10.3389/feart.2022.857854>, 2022.

1259 Yao, T., Bolch, T., Chen, D., Gao, J., Immerzeel, W., Piao, S., Su, F., Thompson,
1260 L., Wada, Y., Wang, L., Wang, T., Wu, G., Xu, B., Yang, W., Zhang, G., Zhao, P., 2022.
1261 The imbalance of the Asian water tower. *NATURE REVIEWS EARTH &*
1262 *ENVIRONMENT* 3, 618–632. <https://doi.org/10.1038/s43017-022-00299-4>

1263 Yao, Y., Zheng, C., Andrews, C. B., Scanlon, B. R., Kuang, X., Zeng, Z., Jeong,
1264 S.-J., Lancia, M., Wu, Y., and Li, G.: Role of Groundwater in Sustaining Northern
1265 Himalayan Rivers, *Geophys. Res. Lett.*, 48, <https://doi.org/10.1029/2020GL092354>,

1266 2021.

1267 [Yin, G.-A., Niu, F.-J., Lin, Z.-J., Luo, J., and Liu, M.-H.: Data-driven](#)
1268 [spatiotemporal projections of shallow permafrost based on CMIP6 across the Qinghai–](#)
1269 [Tibet Plateau at 1 km² scale, *Advances in Climate Change Research*, 12, 814–827,](#)
1270 <https://doi.org/10.1016/j.accre.2021.08.009>, 2021

1271 Zekollari, H., Huss, M., Farinotti, D., and Lhermitte, S.: Ice - Dynamical Glacier
1272 Evolution Modeling—A Review, *Reviews of Geophysics*, 60, e2021RG000754,
1273 <https://doi.org/10.1029/2021RG000754>, 2022.

1274 Zhang, T.: [Influence of the seasonal snow cover on the ground thermal regime: An](#)
1275 [overview, *Reviews of Geophysics*, 43, 2004RG000157,](#)
1276 <https://doi.org/10.1029/2004RG000157>, 2005.

1277 [Zhang, S., Gao, X., Zhang, X., and Hagemann, S.: Projection of glacier runoff in](#)
1278 [Yarkant River basin and Beida River basin, Western China, *Hydrol. Process.*, 26, 2773–](#)
1279 [2781, *https://doi.org/10.1002/hyp.8373*, 2012.](#)

1280 Zhang, T., Li, D., and Lu, X.: Response of runoff components to climate change
1281 in the source-region of the Yellow River on the Tibetan plateau, *Hydrol. Process.*, 36,
1282 <https://doi.org/10.1002/hyp.14633>, 2022.

1283 Zhang, Z., Wang, Y., Ma, Z., and Lv, M.: Response mechanism of soil structural
1284 heterogeneity in permafrost active layer to freeze-thaw action and vegetation
1285 degradation, *CATENA*, 230, <https://doi.org/10.1016/j.catena.2023.107250>, 2023.

1286 [Zhang, Y. and Ma, N.: Spatiotemporal variability of snow cover and snow water](#)
1287 [equivalent in the last three decades over Eurasia, *Journal of Hydrology*, 559, 238–251,](#)
1288 <https://doi.org/10.1016/j.jhydrol.2018.02.031>, 2018.

1289 [Zhu, Y. Y. and Yang, S.: Evaluation of CMIP6 for historical temperature and](#)

1290 [precipitation over the Tibetan Plateau and its comparison with CMIP5, Advances in](#)
1291 [Climate Change Research, 11, 239–251, https://doi.org/10.1016/j.accre.2020.08.001,](#)
1292 [2020.](#)